Master's thesis

NTNU
Norwegian University of Science and Technology
Faculty of Information Technology and Electrical Engineering
Department of Engineering Cybernetics

Viktor Korsnes

Performance evaluation of different Kalman filters for state estimation of lithium-ion batteries

Master's thesis in Cybernetics and Robotics
Supervisor: Jon Are Suul
January 2022

NTNU
Norwegian University of
Science and Technology

Viktor Korsnes

Performance evaluation of different Kalman filters for state estimation of lithium-ion batteries

Master's thesis in Cybernetics and Robotics
Supervisor: Jon Are Suul
January 2022

Norwegian University of Science and Technology
Faculty of Information Technology and Electrical Engineering
Department of Engineering Cybernetics

NTNU
Norwegian University of
Science and Technology

Performance evaluation of different Kalman filters for state estimation of lithium-ion batteries

Author
Viktor Korsnes

Supervisor
Jon Are Suul

January 10, 2022

Department of Engineering Cybernetics

NTNU

Abstract

Lithium-ion batteries represent an enormous industry and is shown to be a cornerstone in reducing greenhouse gasses. As the electrification of the transportation sector continues to increase, the potential gains of extending the life span of lithium-ion batteries are significant. This optimization of life span will only be possible given an adequate estimation of the internal dynamics and state of the battery. One such internal state is the State of Charge.

This thesis will act as a continuation of the project thesis. The project thesis recorded experimental data, and different models were designed and identified. This thesis aims to estimate the state of charge using a model-based estimation technique. The estimation methods implemented and compared are the extended Kalman filter and the central difference Kalman filter.

With these estimation methods, the system manages to correct for a wrong initial state of charge and estimate it within a 5% bound. The relation from the state of charge to the open circuit voltage is also investigated, and two methods are tested, a parametric polynomial and linear interpolation. Real-world data noise can often be a problem, and a zero-phase low pass filter is used with good results.

Sammendrag

Litium-ion-batterier representerer en enorm industri og har vist seg å være en sentral teknologi for å redusere klimagasser. Ettersom elektrifiseringen av transportsektoren fortsetter å øke, vil de potensielle gevinstene ved å forlenge levetiden til litium-ion-batterier være betydelige. Denne optimaliseringen av levetiden vil kun være mulig gitt et tilstrekkelig estimat av den interne dynamikken og batteriets tilstand. En av disse interne tilstandene er batteriets restkapasitet.

Denne oppgaven vil fungere som en fortsettelse av prosjektoppgaven. Prosjektoppgaven hentet inn eksperimentelle data, og ulike modeller ble designet og identifiserte parameterne. Denne oppgaven tar sikte på å estimere batteriets restkapasitet ved hjelp av en modellbasert estimeringsteknikk. Estimeringsmetodene som er implementert og sammenlignet er det utvidede Kalman-filteret og sentral-forskjells-Kalman-filteret.

Med disse estimeringsmetodene klarer systemet å korrigere for en feil initial ladetilstand og estimere den innenfor en grense på 5%. Forholdet fra batteriets restkapasitet til åpen kretsspenning undersøkes også, og to metoder testes, et parametrisk polynom og lineær interpolasjon. Målestøy fra den virkelige verden kan ofte være et problem i eksperimentelle data, og et nullfase lavpassfilter brukes med gode resultater.

Preface

This thesis marks the end of five and half years at NTNU, give or take some months. Three of these years were spent as a member of Revolve NTNU. Being a part of Revolve NTNU was a fantastic experience, and the experiences and knowledge gained there will undoubtedly help me later in life. I would therefore extend my gratitude for Revolve NTNU, the sponsors, NTNU, and last but not least, the teammates and friends from team 2019, 2020, and 2021.

I would also like to thank my supervisor Jon Are Suul, for giving me the guidance and freedom to write this thesis in the way I wanted to.

Contents

List of Tables

List of Figures

Acronyms

BEV Battery Electrical Vehicle. 1

BMS Battery Management System. 1, 66

CDKF Central-Difference Kalman filter. viii, x, 3, 29, 44–48, 54, 58–63, 66

ECM Equivalent Cell Model. 2, 24, 30, 32, 63

EKF Extended Kalman filter. viii, x, 3, 4, 6, 23, 26, 28, 30, 32, 45, 47, 48, 50, 54–58, 60–63, 66

HEV Hybrid Electrical Vehicle. 1

HPPC Hybrid Pulse Power Characterization. 3, 56

LIB Lithium-Ion Battery. ix, 1, 2, 4, 6, 7, 9, 10, 14, 19, 20, 66

LUT Lookup Table. 40, 50, 55, 58, 61

OCV Open Circuit Voltage. x, 4, 6, 8, 10, 11, 14, 32, 33, 39–41, 47–51, 55, 59–61, 63, 65

PDF Probability Density Function. 15

PMF Probability Mass Function. 15

SEI Solid Electrolyte Interface. 10, 11

SoC State of Charge. x, 1–3, 5–11, 19, 32, 33, 39–42, 44, 46–49, 54–61, 63–66

SoH State of Health. 1, 2, 11

SoP State of Power. 66

SPKF Sigma Point Kalman Filter. 3, 6, 26, 28, 29, 32, 45, 56, 60, 63

UKF Unscented Kalman Filter. viii, 3, 29, 45

Chapter 1

Introduction

With the first introduction of battery technology, a fundamental problem has been to estimate the remaining energy [3]. When the automotive industry started using batteries in the tractive systems in the form of Battery Electrical Vehicle (BEV)s and Hybrid Electrical Vehicle (HEV)s, the problem became crucial in order to estimate the available driving range [3]. The current trend for tractive system batteries is Lithium-Ion Battery (LIB)s, which makes monitoring the battery internal states essential, not just for the available range, but also from a safety perspective [4]. Operating the battery pack outside its operating area may have dire consequences [5].

The system which is responsible for estimating the remaining energy, also known as State of Charge (SoC), is the Battery Management System (BMS). Its tasks include, but are not limited to SoC & SoH estimation, safety & protection, charging control, thermal management, and cell balancing [3]. To fulfil these tasks, a BMS has several features to control and monitor the state of the battery at the battery cell level and the entire battery pack. The monitored states are the cell voltage, temperature, and current.

For SoC estimation, there is a multitude of solutions [6]. The primary input to most of these is the current. Although it is possible to use the voltage directly, this will often lead to inaccurate results. The simplest method is to integrate the current over time, known as Coulomb counting. A model-based approach where a mathematical model of the cell is fed the current as input allows the introduction of the voltage measurements in the form of a filtering method [7].

The electrification of the transportation section has been identified as a crucial component to reduce humanity's greenhouse gas emissions [8]. Batteries act as a green revolution to the internal combustion engine and a potentially essential part of the smart energy grid [3]. With the performance from LIBs stagnating, the ability to optimize the life span will be very important, as a small increase leads to a large global effect [9]. This is where SoH comes in, and an important step for SoH estimation is a accurate SoC estimate.

1.1 Background

This thesis build upon the project thesis[10]. In where a test regime was developed and executed on a **Lithium Cobalt Oxide** pouch cell. Additionally the experimental data was used to create parameters for Equivalent Cell Model (ECM) using the Matlab product, Simulink Design Optimization [11]. The workflow of the project thesis is visualized in fig. 1.1.

1.2 Strategy

Once the model was set up in Simulink, the current was fed into the model, and the paramaters were optimized such that the square of the measured value minus the model output was minimized. Resulting from the project thesis was a set of model parameters ($\boldsymbol{\theta}(z(t))$ that changes with the SoC

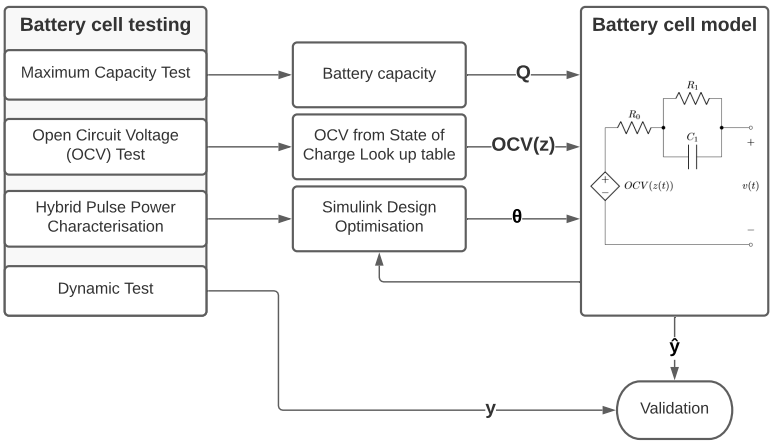

Figure 1.1: The strategy of the project thesis which built the foundations of this thesis.

($z(t)$). All of the parameters was trained using a Hybrid Pulse Power Characterization (HPPC), and in order to validate the performance a dynamic load cycle was used.

The parameters and experimental data gives a good foundation for implementing and validating different Kalman filters. The reason for implementing the filtering methods is in order to correct for a bad initial SoC when the system starts up, and correct for drift as the system runs.

1.3 Strategy and structure

The goal of this thesis is to implement and validate two different nonlinear Kalman filters. An Extended Kalman filter (EKF) and a Sigma Point Kalman Filter (SPKF). Two different SPKF will be presented, the Unscented Kalman Filter (UKF) and Central-Difference Kalman filter (CDKF), and the latter is the one that will be implemented. In order to narrow the workload it will only be implemented one of the models from the project

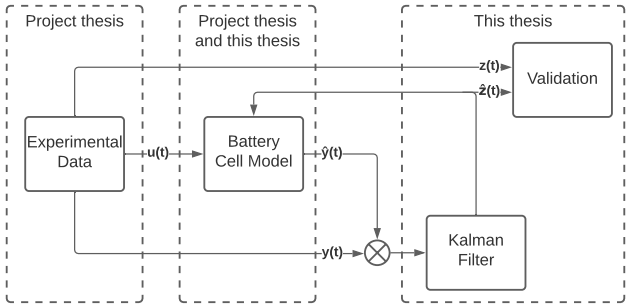

Figure 1.2: The work performed in this thesis.

thesis. The Open Circuit Voltage (OCV) curve will also be revisited, as the EKF requires the derivatve of the OCV curve, which needs some processing in order to attenuate the noise.

The thesis will start with the necessary theory in order to understand the Kalman filter and the battery model. By first introducing the governing principles for a LIB and then building up the foundation for Kalman filtering starting from basic statistics. Once the reader has enough knowledge and understand the goal of a battery model, the battery modelling will be briefly described. Next, the application of the chosen battery model in the framework of a EKF are shown, before the final section mainly describes the theory behind the updated OCV curve.

Before introducing the results a short interlude on the methodology used for the results will presented. The methodology section will present the way the experiments has been set up. Finally the results will be discussed and a conclusion will be drawn based on the results and the theory.

The results of the thesis are briefly summarized in fig. 1.2

1.4 Contribution

The author performed the collection of experimental data in [10]. The modelling is adapted mainly from [12], with the parameter identification performed by the author in [10].

This thesis adopts the implementation of the filters from [1] with a model and parameters from [10]. In other words, this thesis performs SoC on lithium cobalt oxide batteries with very demanding load cycles. Figure 1.2 illustrates the contributions with regards this thesis and the project thesis.

Chapter 2

Theory

This chapter will start by explaining some of the governing principles in LIBs and then explain the different Kalman filters. The thesis will establish a foundation from basic statistics, random processes, and Kalman filters. As mentioned in the preamble, two filters will be investigated: EKF and SPKF. The following section goes through the adaption of these filters to a LIB model. Essential tools when applying the Kalman filters to the LIB are curve fitting and derivatives.

2.1 Lithium-ion batteries working principle

To model LIBs, a rudimentary knowledge of the internals is necessary. This section will briefly describe the working principles of a LIB with a focus on what is the most important properties for this thesis. The most important factors when modelling is the SoC, OCV and polarizing voltages. To understand these terms, some basic principles within electrochemistry are necessary.

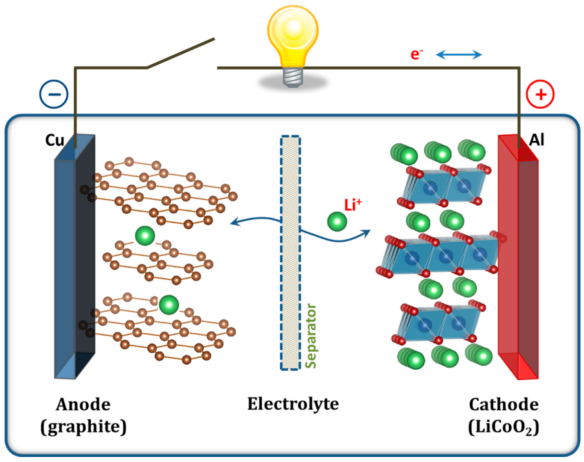

Figure 2.1: A schematic illustration of a Cobalt Oxide LIB[13]

2.1.1 A brief introduction to electrochemistry

In fig. 2.1 the innards of a LIB is shown. This model has a lithium cobalt oxide cathode and a graphite (carbon) anode. The cathode and anode are electrodes and will be defined as the positive and negative electrodes, as the role of anode and cathode changes depending on the direction of the current. The naming is summarised in table 2.1.

The idea is that by exerting an external electrical field onto the electrodes such that the negative electrode experiences an elevated potential compared to the positive electrode, the lithium ions will flow from the positive to the negative electrode. When the battery is fully charged, the negative electrode will be saturated with lithium ions in the sense that adding more can significantly affect aging [14], or worse, initiate a thermal runaway [15]. In the other direction, when discharging, the electrodes are connected through a load, and the lithium ions will flow the other way into the positive electrode, with the electrons flowing in the external circuit.

The percentage of lithium in the negative electrode is what decides the SoC. When the electrode receives or relinquishes lithium, the electrode as

a whole will change its *electrode potential*. It is this potential difference between the electrodes that define the OCV.

Table 2.1: Terminology of electrodes.

Electrode	Charging	Discharging
Negative electrode	Cathode	Anode
Positive electrode	Anode	Cathode

2.1.2 Electrochemical impedance

When a cell discharges, it will be a voltage drop when measuring the terminal voltage. Similarly, there will be a voltage rise in the terminal voltage when charging. The OCV will only change based on the SoC change. The terminal voltage, $v(t)$, is the voltage that would be measured at the battery cell poles, and with the OCV as U_{ocv}, the voltage drop can be defined as

$$U_P = U_{ocv} - v(t),$$

where U_P is the *polarizing* voltage. This polarization voltage will be further elaborated on in section 2.1.7.

2.1.3 C-rate

C-rate is a measure of the rate at which a battery is being charged or discharged. $1C$ is defined as the current the battery could maximum deliver in one hour with its nominal rated capacity. The battery will be empty after discharging it with a current of $1C$ for one hour. Note that even though a $20C$ rate should empty the battery in 3 minutes, this will most certainly not be the case due to Peukert's law [16]. In addition, a larger current will lead to a larger polarizing voltage leading to reaching the lower cut-off voltage before the battery is fully discharged.

2.1.4 State of Charge

As stated previously, the lithium concentration in the negative electrode (and consequently in the positive electrode) decides the SoC. The LIB manufacturer defines an upper and lower voltage limit on the cell. However, this can be bypassed with extensive testing [17], if the cell is shown by experiments to safely be able to store more energy and handle the increased voltage.

The SoC is defined by these limits set by the manufacturer or experiments. The battery cell is fully charged when relaxed, and the terminal voltage reads approximately the upper limit. Conversely, when the cell is relaxed, and the terminal voltage reads approximately the lower limit, the cell is fully discharged.

In order to relate the fully charged and fully discharged state, the cell's capacity is needed. Due to the effect of Peukert's law, the capacity will depend on the C-rate chosen to measure the capacity. The cell manufacturer defined the capacity given a certain C-rate [16]. The test usually discharges because charging introduces some side effects, which are denoted by the *Coulombic efficiency* [18]. The Coulombic efficiency is usually denoted by η, but the effect is small and would only cause a slight drift of the value while charging.

Once these values are all known the change in SoC can be modelled as such

$$\dot{z}(t) = z(t_0) - \frac{1}{Q}\int_{t_0}^{t_1} \eta(t) i(t) dt, \tag{2.1}$$

where z denotes the SoC, Q is the capacity and $i(t)$ is the applied current. This describes the SoC from a point in time, t_0, until a future point in time t_1.

2.1.5 State of Health

The two main factors that lead to performance loss and inevitably the end of life for a LIB are the capacity and power fade. Capacity fade is the process where the LIB receives a reduced capacity and is mainly due to the loss of cyclable lithium and active materials in the electrodes. These are results of unwanted side reactions in the cell and can, to some degree, be blamed on the growth of the Solid Electrolyte Interface (SEI). The SEI is a vital layer that forms on the electrode surface, in the interface between the electrode and electrolyte. This layer forms on the negative electrode during the battery's first charging cycle. By doing the first charging cycle in a controlled environment with a low current, the SEI becomes densely packed[19] and thus hinders the decomposition of the graphite into the electrolyte. However, over time this layer will continue to grow. The layer is created by incapacitating lithium, which reduces the cell's capacity. Another issue is that the impedance of the cell increases. When the impedance increases, the current capabilities decrease due to the voltage drop. This phenomenon is known as power fade. For a more comprehensive overview of these aging mechanisms, see [20].

2.1.6 Open circuit voltage

The Open Circuit Voltage (OCV) is formally defined as

$$U_{ocv} = u^{+}_{ocp} - u^{-}_{ocp} \tag{2.2}$$

where U_{ocv} is the OCV while $u^{\cdot}_{ocp}$ is the *open circuit potential* of the positive and negative electrode, respectively. As mentioned previously, the potential is a function of lithium concentration in the specific electrode. The OCV is the equilibrium point of the cell at a given SoC when neglecting self discharge and other phenomenons acting over a large time horizon.

Establishing a relationship between the OCV and SoC can be done with testing. The common way to do this is by dividing the SoC into discrete steps, for example, 20, such that there is one point for each 5%. Next, the cell is fully charged, left to rest for a long time, and then the voltage is logged. The cell is then discharged a 20th part, and the procedure is repeated. Berckmans et al. [21] used a method called quasi-open circuit voltage. This method discharges/charges the cell at a small current, where the idea is that the cells will be at equilibrium the entire cycle. In the previous work, a current of $\frac{C}{30}$ was used.

In addition to lithium concentration, the potential of the electrodes is also dependant on the temperature [22]. Therefore the experiments are often performed in controlled conditions and repeated at different temperatures. In addition to SoH the relationship also depends on pressure[23] and a hysteresis effect [24] further complicates the modelling.

The modelling of the OCV-SoC relationship is also found to be crucial when it comes to battery State of Health (SoH) monitoring, as OCV data often reflect battery aging and performance degradation [25]. This is also what makes it difficult to model the relationship, as it depends on the SoH which is difficult to model without an abundance of test data over the battery cell life cycle [26].

2.1.7 Polarizing voltages

Another way to visualize the polarising voltages is through a Nyquist diagram of the impedance response. In fig. 2.2 such a response can be seen. A negative imaginary impedance is a capacitive impedance, and a positive imaginary value is an inductive load. At very high frequencies, the inductance in the current collectors and wiring becomes dominating. The first part of the capacitive impedance is the SEI, which is usually merged into the charge transfer, as it plays a minor part. At least on relatively new cells

[19]. The charge transfer can resemble a subdued semicircle [27]. Furthermore, diffusion, or mass transport as it is named here, resembles a straight line.

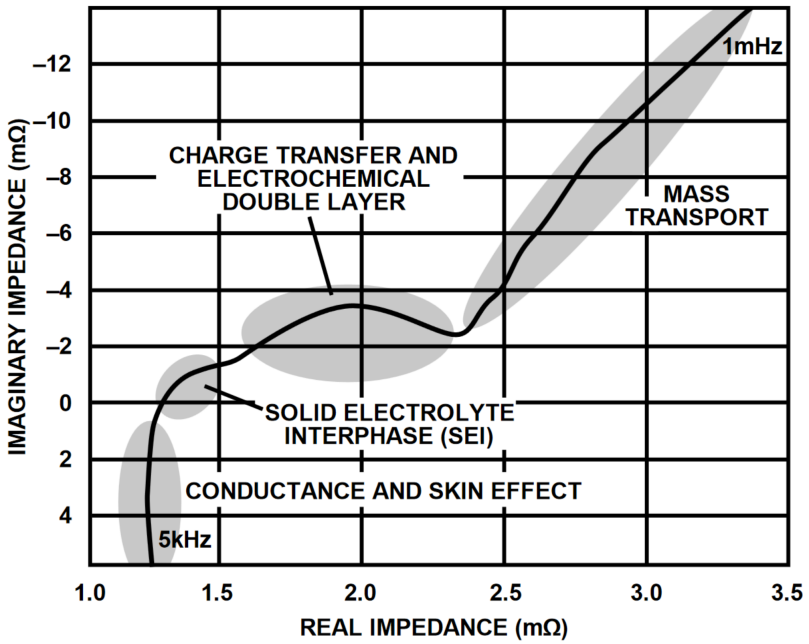

Figure 2.2: Nyquist plot for a battery showing the different regions corresponding to an electrochemical process [28]

In the following section, the previously defined terms are related to an actual voltage response. In fig. 2.3 the R_0 is the ohmic impedance and can be thought of as the resistance through the cell, i.e., if you were to measure the cell at a relaxed state, this is the quantity you would measure. The $R_{CT}(\omega)$ is the charge transfer impedance. This is due to the charge building upon the electrodes at the interface to the electrolyte. This quantity can only be observed when the cell is under a load and will go back to chemical energy once the cell goes back to a relaxed state. $R_P(\omega)$ is the diffusion impedance, and it arises due to the lithium concentration in the electrode surface decreasing, the lithium ions have to travel further. Once the cell relaxes, the concentration gradient of lithium in the electrode will commingle. Note that the charge transfer and diffusion are dependant on frequency while the ohmic is not.

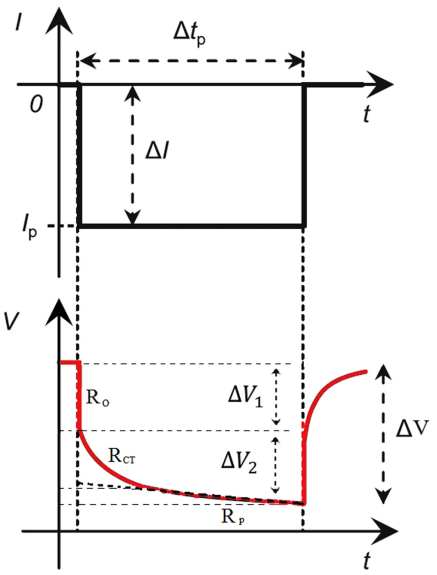

Figure 2.3: The upper plot shows the applied current pulse, while the lower plot shows the voltage response. The figure shows how the entire polarizing voltage (ΔV) is a sum of the ohmic voltage drop (ΔV_1) and the (ΔV_2), the voltage drop due to diffusion is negligible on such a short time interval [29].

These three phenomenons are listed in the order of their timescales. The ohmic impedance is instantaneous, the charge transfer activates within a few seconds, and the diffusion can take much longer. Summed, they compose the polarization voltage. The charge transfer and diffusion do not only introduce an impedance which creates a voltage drop but also affect the voltage when the current is switched off, as seen in the lower part of

fig. 2.3.

The inductive and capacitive impedance is reactive. This means that once the current through the cell is removed, the energy spent *activating* these different loads will to some degree, go back to being chemical energy. The effect this has on the terminal voltage of the cell is called *polarising*. Polarizing refers to any voltage deviance from the OCV due to memory effects from the applied current on the LIB. In order to model the polarising effects, a good impedance model will be necessary.

2.2 Description of a random process

This paper introduces filtering techniques for a more accurate estimation of various states within the LIB from noisy measurements. Before proceeding with the filtering, it is necessary to describe the nature of noise. This section will start with some simple results from probability theory before venturing onto white Gaussian noise and Brownian motion.

2.2.1 Probability theory and random variables

The probability of an event A will be denoted $P(A)$. The following definition gives the conditional probability:

$$P(A|B) = \frac{P(A \cap B)}{P(B)}, \tag{2.3}$$

where A and B are to events and $A \cap B$ denotes the event that A *and* B happens. Another important definition is independence which if the following holds

$$P(A|B) = P(A), \quad P(B|A) = P(B), \tag{2.4}$$

the events are independent.

The entire sample space gets a special symbol, Ω. By partitioning Ω into a countable class B_n and given an event A the following sum will result in probability

$$P(A) = \sum_n P(A \cap B_n) = \sum_n P(A|B_n)P(B_n). \tag{2.5}$$

Finally the backbone of all Bayesian filtering, Bayes' rule is stated:

$$P(A|B) = \frac{P(B|A)P(A)}{P(B)} \Leftrightarrow Posterior = \frac{Likelihood \times Prior}{Normalization}. \tag{2.6}$$

Bayes' rule opens up for Bayesian filtering, which is a form of *optimal* filtering formulated in the Bayesian framework. Optimal refers to the filter being statistically optimal when filtering a signal corrupted by noise. More on this in section 2.3.

Probability mass and density functions describe discrete and continuous probability distributions, respectively. A Probability Mass Function (PMF) has a countable sample space, while a Probability Density Function (PDF) has an uncountable sample space. The Gaussian random variable is an example of a PDF and has the following form

$$N(x; \mu, \sigma) = \frac{1}{\sigma\sqrt{2\pi}} exp\left(-\frac{1}{2}\frac{(x-\mu)^2}{2\sigma^2}\right), \tag{2.7}$$

where μ is the expected value of $f(x)$ and σ^2 is the variance. The expected value is the theoretical outcome on average as the number of experiments goes to infinity. The variance is a measure of the spread of the data. A high variance means the data is more spread out, and extreme values will be more likely. A low variance on the other side means that the data will be less spread, and extreme values are less likely to be observed.

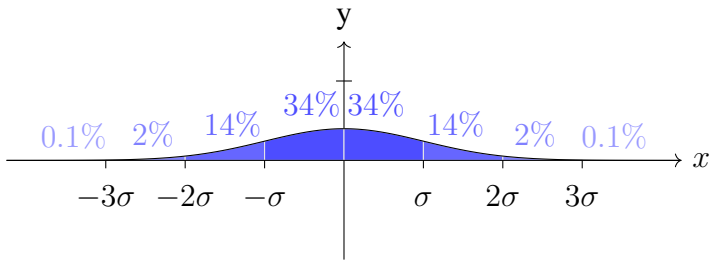

Figure 2.4: An illustration of the variance in a Gaussian distribution. The percentages describe how much data is within the different sigma limits. The 3σ limit will contain 99.7% of the data.

2.2.2 The multivariate Gaussian distribution

The Gaussian distribution has some excellent computational properties, which makes it possible to find closed-form solutions when adding and multiplying the Gaussian's [30]. The univariate Gaussian from eq. (2.7) can be generalized to the multivariate version by exchanging the mean μ with a vector of means, $\boldsymbol{\mu}$. The variance σ will be a matrix $\boldsymbol{\Sigma}$ which contains the variance of each random variable on the diagonal and the cross-correlation on the off-diagonal elements. Due to the cross-correlation being a symmetric relation, the covariance matrix must also be symmetric [30]. It is also a positive semi-definite matrix, which intuitively can be thought of as a negative variance is impossible. The formula can be seen in the following equation:

$$N(\boldsymbol{x}; \boldsymbol{\mu}, \Sigma) = \frac{1}{(2\pi)^{\frac{n}{2}}|\Sigma|^{\frac{1}{2}}} exp\left(-\frac{1}{2}(\boldsymbol{x}-\boldsymbol{\mu})^T\Sigma^{-1}(\boldsymbol{x}-\boldsymbol{\mu})\right). \tag{2.8}$$

Without going into the proofs, the following properties hold for the multivariate Gaussian [31]:

- A multivariate Gaussian distribution is still Gaussian after an affine transformation.

- The conditional distribution of two Gaussian distributions is Gaussian.
- The marginal distribution of a jointly Gaussian distribution is still Gaussian.
- The sum and difference of two Gaussian distributions are still Gaussian, given that they are independent.

2.2.3 Stochastic processes

A stochastic process is an ensemble of random variables. Each realization of a stochastic process is a function. In other words, if a space of all valid functions for the stochastic process is defined, a realization will be a point(function) in this space. A typical discrete stochastic process is the random walk. The random walk in one dimension models the behavior of a particle in which the distance moved between time steps is a random variable. The process can then be used to give parameters of a model the flexibility to change. In other words, by modelling the parameters as a random variable, the Kalman filter can push the parameters in the statistically optimal direction. If the random variable deciding the displacement is a Gaussian, the walk is called a Gaussian random walk. Having a Gaussian random walk makes it easy to tune the volatility of the parameter. By increasing sigma, the parameter is likely to make more significant steps.

A mathematical model of one-dimensional Gaussian random variable has the following form

$$x[0] = x_0 \tag{2.9}$$

$$x[k+1] = x[k] + \mathcal{N}(\mu, \sigma) \tag{2.10}$$

where μ is usually zero. From this formulation, the μ can be thought of as a

bias, while the σ gives the uncertainty. For example, modelling something that degrades over time would probably give better results with a bias to the random walk. It is also possible to make the bias and uncertainty time-dependent. It makes sense to decrease the uncertainty if the initial guess is non-optimal and the system gets consistently closer to the true model. In other words, if the system has a consistent filter [30].

2.2.4 Statistical approximations

Although modelling a random variable as Gaussian is a simplification, but as mentioned in section 2.2.2 it has some remarkable properties which will make the filtering algorithm much simpler. It will also allow a closed form solution for the Kalman filter.

Approximating a Gaussian from a set of samples usually involves calculating the mean and the covariance given some method or weighing the points. It also includes the case where the process itself is not strictly Gaussian but is assumed Gaussian due to the aforementioned reasons.

A non-linear transformation of a Gaussian distribution is, in most cases, not a Gaussian after the transformation. A Gaussian can be approximated after the transformation using many solutions. Points from the original distribution can be generated, then propagated through the non-linear function. Afterward, they can be reconstructed into a Gaussian [32]. The main issue with this is that it potentially requires a large amount of computational power. Another issue that is more related to the Gaussian itself is that it can only handle unimodal systems[31], that is, a single peak. Regarding the computational issue, a solution exists. The unscented transformation.

2.3 Filtering

In the context of filtering in this paper, the goal is to estimate the current value given past and current observation. The obvious observation with regards to battery estimation is the voltage. However, the goal is often to estimate a *hidden* state, SoC. Thus the observations, given as voltage measurements, must be related to the SoC through what is often referred to as the measurement equation.

An important assumption for many filtering algorithms and indeed every technique in this thesis is the Markov assumption. In simple terms the Markov assumption in a discrete system with a state vector and a observation, the current state relies only on the previous state, and similarly the observation must only depend on the current state. From a probabilistic framework the they can be formalised as

$$p(\boldsymbol{x}_k|\boldsymbol{x}_1, \ldots, \boldsymbol{x}_{k-1}, \boldsymbol{y}_k, \ldots, \boldsymbol{y}_{k-1}) = p(\boldsymbol{x}_k|\boldsymbol{x}_{k-1}), \tag{2.11}$$

$$p(\boldsymbol{y}_k|\boldsymbol{x}_1, \ldots, \boldsymbol{x}_k, \boldsymbol{y}_k, \ldots, \boldsymbol{y}_{k-1}) = p(\boldsymbol{y}_k|\boldsymbol{x}_k), \tag{2.12}$$

Where $\boldsymbol{x}_k$ denotes the state and $\boldsymbol{y}_k$ the observation. If these assumptions did not hold, the equations would grow linearly with time and become intractable.

The goal of filtering with application to LIB then becomes to estimate the internal state of the LIB given the voltage measurements. This is illustrated in fig. 2.5. Note that extending the state vector to include other internal variables in the cell is possible. By turning a parameter into a time varying state, e.g., by modelling as a random walk, the state vector can be augmented to include the additional states.

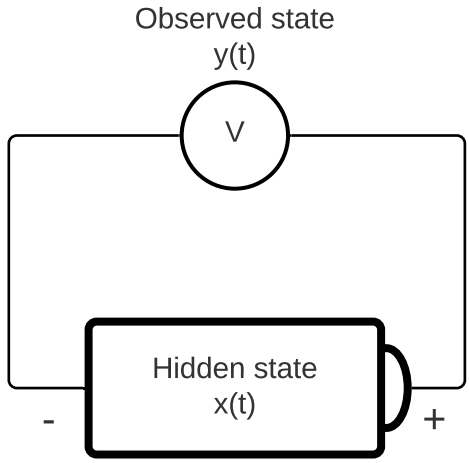

Figure 2.5: The relation between the state and observation in LIB

2.3.1 Bayesian estimation

Bayesian estimation attempt to compute the hidden states $\boldsymbol{x}_{0:k}$ where the notation $_{0:k}$ denotes the time series from $\boldsymbol{x}_0, \ldots, \boldsymbol{x}_k$, from the observed measurements $\boldsymbol{y}_{1:k}$. Under the Markov assumption the joint probability simplifies greatly to

$$p(\boldsymbol{x}_{0:k}, y_{1:k}) = p(\boldsymbol{x}_0) \prod_{i=1}^{k} p(\boldsymbol{y}_i|\boldsymbol{x}_i) p(\boldsymbol{x}_i|\boldsymbol{x}_{i-1}). \tag{2.13}$$

Equation (2.13) calculates the entire joint probability. However, when filtering, the probability distribution of interest is associated with the current states conditioned on the measurements up to the current time step. This leads to the backbone of all the methods used in this thesis: the *predict* and *update* step.

The prediction step, also known as the Chapman-Kolmogorov equation,

follows from the total probability theorem and is given by

$$p(\boldsymbol{x}_k|\boldsymbol{y}_{1:k-1}) = \int p(\boldsymbol{x}_k, \boldsymbol{x}_{k-1}|\boldsymbol{y}_{1:k-1})d\boldsymbol{x}_{k-1}. \tag{2.14}$$

The update is proportional to the product of the measurement likelihood and the predicted state, and given by

$$p(\boldsymbol{x}_k|\boldsymbol{y}_{1:k}) = \frac{p(\boldsymbol{y}_k|\boldsymbol{x}_k)p(\boldsymbol{x}_k|\boldsymbol{y}_{1:k-1})}{p(\boldsymbol{y}_k|\boldsymbol{y}_{1_k-1})} \propto p(\boldsymbol{y}_k|\boldsymbol{x}_k)p(\boldsymbol{x}_k|\boldsymbol{y}_{1:k-1}) \tag{2.15}$$

Where the factors are denoted:

- $p(\boldsymbol{x}_k|\boldsymbol{y}_{1:k-1})$ - Prediction
- $p(\boldsymbol{x}_k|\boldsymbol{y}_{1:k})$ - Update
- $p(\boldsymbol{y}_k|\boldsymbol{x}_k)$ - Likelihood
- $p(\boldsymbol{y}_k|\boldsymbol{y}_{1_k-1})$ - Normalisation

These two equations, eq. (2.14) and eq. (2.15) together makes up the Bayes filter and is illustrated in fig. 2.6

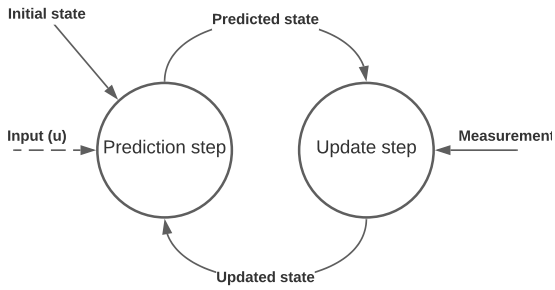

Figure 2.6: The recursive nature of the Bayes filter visualised

2.3.2 Kalman filter

A classic and much used filtering technique is the Kalman filter. The Kalman filter is a special case of the Bayes filter, where both the process

and measurement models are Gaussian and linear. In that case, the Bayes filter will have a closed-form solution, and in addition, it will also be the optimal solution. Here optimal refers to the fact that the Kalman filter will be the minimum mean square error estimator, which in mathematical terms is formulated as

$$\hat{x}_{MMSE}(y) = argmin_{\hat{x}} MSE = E\{x|y\}, \tag{2.16}$$

where $\hat{x}$ denotes the estimator.

When applying the Kalman filter, the state reduces to a Gaussian random variable, which can be parameterized as a vector of means and a covariance matrix. The mean values are the expected state values, and the covariance matrix introduces an uncertainty value of the different states. This can in turn, be used to create an error bound on our estimates. An example of this is shown in fig. 2.7 where an arbitrary state from one of Matlabs many examples are plotted together with the 1σ bound [2].

The most critical property for the residuals is that they appear to be white noise with zero mean.

2.3.3 Extended Kalman filter

The Kalman filter, as mentioned, requires that the models are linear, which in many cases is sufficient, and the model is or can be linearized around a particular point. Compared to the standard Kalman filter, the extended is a Taylor approximation. By assuming that the noise is additive, i.e.

$$\boldsymbol{x}_k = \boldsymbol{f}(\boldsymbol{x}_{k-1}, \boldsymbol{u}_k) + \boldsymbol{q}_{k-1}, \tag{2.17}$$

$$\boldsymbol{y}_k = \boldsymbol{h}(\boldsymbol{x}_k, \boldsymbol{u}_k) + \boldsymbol{r}_k, \tag{2.18}$$

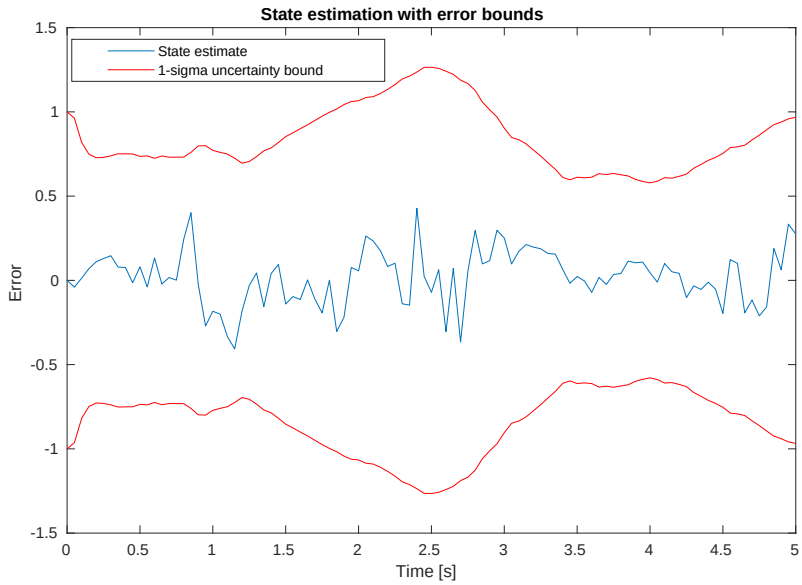

Figure 2.7: A state plotted together with its 1σ error bounds gathered from Matlab example code [2].

where $\boldsymbol{x}_k \in \mathbb{R}^n$ is the state, the $\boldsymbol{u}_k \in \mathbb{R}^d$ is the input and $\boldsymbol{y} \in \mathbb{R}^m$ is the measurement. The $\boldsymbol{q}$ and $\boldsymbol{r}$ represent zero mean Gaussian noise with covariance matrices $\boldsymbol{R}$ and $\boldsymbol{Q}$. Usually, the additive noise is modelled as static processes, and thus the subscript can be omitted. The significance of these assumptions should not be understated. In essence, it claims that $E[f(x)] = f(E[x])$ which is generally not true and is one of the reasons why the EKF in general performs worse the more non-linear the system is. The more quantifiable reason for the reduced performance is because the Taylor series is truncated only to contain the first two terms. The linear terms.

With the assumptions in eq. (2.17) the next step is to linearize the system. This thesis will gloss over the details and present the needed matrices to implement the filter. For a detailed derivation [32]. The following notation will be used

- A Superscript "$-$", x^- indicates a predicted value.
- A Superscript "$+$", x^+ indicates a estimated value, which is updated based on current measurement.
- A hat, $\hat{x}$ indicates an estimate.
- A tilde, $\tilde{x}$ indicates an error, i.e. $\tilde{x} = x - \hat{x}$
- A bar, $\bar{x}$ indicates the mean value of x.

$$\hat{A}_k = \left.\frac{\partial f\left(x_k, u_k\right) + q_k}{\partial x_k}\right|_{x_k = \hat{x}_k^+} \tag{2.19}$$

$$\hat{B}_k = \left.\frac{\partial f\left(x_k, u_k\right) + q_k}{\partial q_k}\right|_{q_k = \bar{q}_k} \tag{2.20}$$

$$\hat{C}_k = \left.\frac{\partial h\left(x_k, u_k\right) + r_k}{\partial x_k}\right|_{x_k = \hat{x}_k^-} \tag{2.21}$$

$$\hat{D}_k = \left.\frac{\partial h\left(x_k, u_k\right) + r_q}{\partial r_k}\right|_{r_k = \bar{r}_k} \tag{2.22}$$

eq. (2.19) is the linearized state matrix, eq. (2.20) is the linearized input matrix, eq. (2.21) is the linearized output matrix and eq. (2.22) is the linearized feed through matrix [33]. In section 2.4.1 these will be derived for a ECM.

In this formulation, the noises are scalar. There is a process noise on the current input, which quantifies the current measurements' noise and, in addition, it also encompasses the modelling noise. The other noise vari-

able is the voltage measurement, which is more tangible than the process noise. The voltage measurement can be defined - at least initially - using the datasheet of the voltage measurement. Finally, the initial covariance of the state vector must be chosen. The method of finding good values for these will be further investigated in the methodology chapter. However, there are a few general guidelines.

An essential aspect of tuning the filter is whether the ground truth is available. If the ground truth is available, it is possible to apply residual analysis to check that the residuals appear to be generated from a white noise process. If the residuals are white noise, it means that there is nothing less to be gained from tuning/modelling. Another desired characteristic is that the residuals should be zero mean.

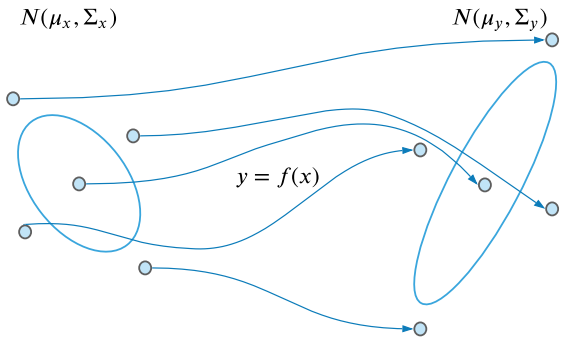

Figure 2.8: Visualisation of the unscented transformation, on the left side you see the carefully chosen sigma points, on the right side you see them after the nonlinear transformation $f(x)$.

2.3.4 Unscented transform

The unscented transformation is visualised in fig. 2.8. The unscented transform defines a systematic way to choose the points to be propagated through a nonlinear transformation and then be reconstructed to create an approximate Gaussian. This differs from using a linearized version of $f(x)$ as can

be seen in fig. 2.9.

The EKF takes a nonlinear function and partial distribution information of the state of a system but applies an approximation to the known function rather than to the imprecisely-known probability distribution. A better approach would be to use the exact nonlinear function applied to an approximating probability distribution.[34]. So the difference in a sense is that neither solution knows the posterior, but the EKF approximates the nonlinear function such that it is a simple affine transformation. However, the unscented transformation makes no approximation and uses the full accuracy of the nonlinear transformation. It can then construct the posterior from imperfect knowledge of the distribution.

2.3.5 Sigma point Kalman filter

The EKF is a great tool, but as mentioned, it has its issues when the system embodies very nonlinear behavior. By introducing the SPKF, a statistical linearization can be used instead.

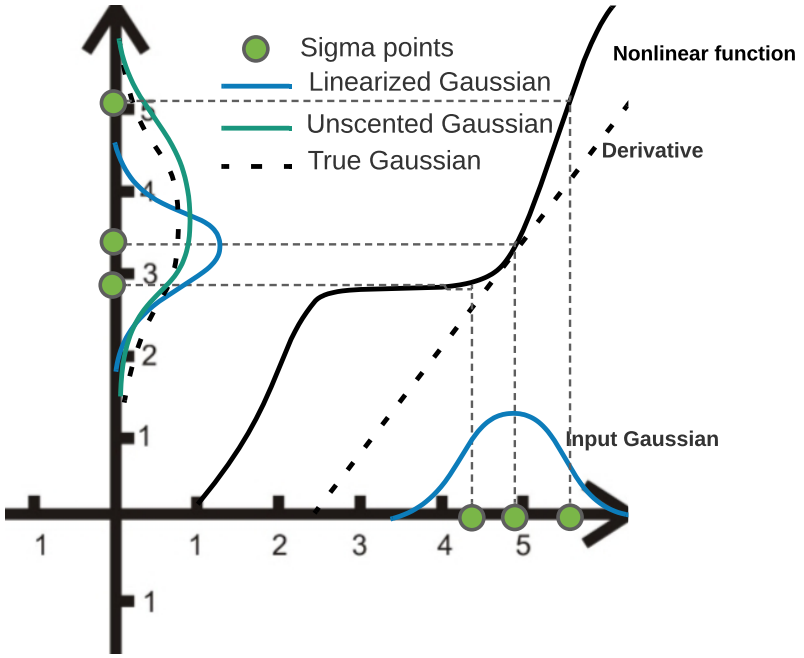

Figure 2.9: In this figure, an example of the unscented transform compared to traditional linearization is shown. The nonlinear function has a very gentle rise before the linearized point and steep after. The unscented transformation accounts for this by putting two sigma points close together and the last far away from the rest. This gives a more reasonable result compared to the linearization. This example is adopted from [1].

There are in general six steps linked to the SPKF method.

1. State-estimate time update.
2. Error-covariance time update.
3. Output estimate.
4. Estimator gain matrix.
5. State-estimate measurement update.
6. Error-covariance measurement update.

Which are the same broad steps as in the EKF, but the differences become clear already at the first step. When generating the sigma points, all the input distributions are combined into a single augmented state vector $\boldsymbol{x}_k^a$ and covariance $\Sigma_{\boldsymbol{x}_k^a}$, where

$$\boldsymbol{x}_k^a = \begin{pmatrix} \boldsymbol{x}_k \\ \boldsymbol{q}_k \\ \boldsymbol{r}_k \end{pmatrix}, \qquad \Sigma_{\boldsymbol{x}_k^a} = \begin{pmatrix} \Sigma_{\tilde{\boldsymbol{x}},\boldsymbol{k}} & 0 & 0 \\ 0 & \Sigma_{\tilde{\boldsymbol{q}}} & 0 \\ 0 & 0 & \Sigma_{\tilde{\boldsymbol{r}}} \end{pmatrix},$$

where the process noise is defined as $\mathcal{N}(\boldsymbol{q}_k, \Sigma_{\tilde{\boldsymbol{q}}})$ and the measurement noise as $\mathcal{N}(\boldsymbol{r}_k, \Sigma_{\tilde{\boldsymbol{r}}})$. Using this distribution, a set of sigma points are generated and split into three sets, one for each group in $\boldsymbol{x}_k^a$. For each set $2n+1$ points will have been generated, where $\boldsymbol{x}_k^a \in \mathbb{R}^n$. Once these sigma points are generated, they can be used to generate the state prediction and covariance, the estimator gain, and the measurement update state and its covariance. For details of the next steps, see [35].

Although this chapter has focused mostly on the unscented transform, it is a sigma point method. There are several different methods to select the sigma points and reassemble them after a transformation [32]. The SPKF are Kalman filters that uses the methods of propagating carefully chosen

	γ	$\alpha_0^{(m)}$	$\alpha_k^{(m)}$	$\alpha_0^{(c)}$	$\alpha_k^{(c)}$
CDKF	h	$\frac{h^2-L}{h^2}$	$\frac{1}{2h^2}$	$\frac{h^2-L}{h^2}$	$\frac{1}{2h^2}$
UKF	$\sqrt{L+\lambda}$	$\frac{\lambda}{L+\lambda}$	$\frac{1}{2(L+\lambda)}$	$\frac{1}{L+\lambda}+(1-\alpha^2+\beta)$	$\frac{1}{2(L+\lambda)}$

Table 2.2: Formulas to calculate the sigma point weights for UKF and CDKF.[1]

(sigma) points through the non-linear function. In this thesis, two variations of the SPKF will be introduced, namely the Unscented Kalman Filter (UKF) and the Central-Difference Kalman filter (CDKF). Note that the only way they differ is in the weighting constants. The difference can be seen in table 2.2. This table requires some explanation.

Given a set of L sigma points $\boldsymbol{\mathcal{X}}$ the mean value is calculated as

$$\bar{\boldsymbol{x}} = \sum_{i=0}^{n} \alpha_i^{(m)} \boldsymbol{\mathcal{X}}_i,$$

and the covariance using the following formula

$$\Sigma_{\tilde{\boldsymbol{x}}} = \sum_{i=0}^{n} \alpha_i^{(c)} (\boldsymbol{\mathcal{X}}_i - \bar{\boldsymbol{x}})(\mathcal{X}_i - \bar{\boldsymbol{x}})^T.$$

The UKF has the following tuning factors λ, α and β where λ is decided by the following equation

$$\lambda = \alpha^2(L+\kappa) - L, \tag{2.23}$$

where κ is another tuning parameter. α and κ decides the spread of the sigma points around the mean. β is used to prior belief on the distribution[36]. If the distribution is Gaussian, $\beta = 2$ [1].

The CDKF on the other hand, only has one tuning variable h, which by setting equal to $\sqrt{3}$ assumes a Gaussian distribution.

2.4 Lithium-ion battery modelling

Based on the previous work, an Equivalent Cell Model (ECM) with series resistance and four resistor-capacitor circuits. The results from the different models from the previous work can be seen in section 2.4. In this table, the 4-RC model performs the best, except for the enhanced self-correcting model [37], but due to that model adding hysteresis, this thesis has opted for the 4-RC model. The resistor-capacitor circuits are completely decoupled, so adding more of them is straightforward. Even though the computational complexity increases. For details about the proposed models, see [10].

Model	RMSE
0-RC	23.00
1-RC	12.60
2-RC	19.94
3-RC	10.73
4-RC	10.00
ESC 2-RC	10.83
ESC 4-RC	9.22

Table 2.3: RMSE values for the different models collected from the project thesis [10].

The model, fig. 2.10 will simply be stated in this thesis, for details on deriving it see [10] or [12]. In order to forshadow the EKF implementation, the model is stated with the process noise, $q[k]$ added to the current, and measurement noise $r[k]$ to the measurement equation.

The state equation:

$$\underbrace{\begin{pmatrix} z[k+1] \\ \boldsymbol{i}_R[k+1] \end{pmatrix}}_{x_{k+1}} = \underbrace{\begin{pmatrix} 1 & 0 \\ 0 & A_{RC} \end{pmatrix}}_{A} \underbrace{\begin{pmatrix} z[k] \\ \boldsymbol{i}_R[k] \end{pmatrix}}_{x_k} + \underbrace{\begin{pmatrix} -\frac{\Delta t}{Q} \\ B_{RC} \end{pmatrix}}_{B} \underbrace{(i[k] + q[k]),}_{u_k} \quad (2.24)$$

where

$$\boldsymbol{i}_R = \begin{pmatrix} i_{R_1} \\ i_{R_2} \\ i_{R_3} \\ i_{R_4} \end{pmatrix}$$

describes the current through each resistor except R_0, and the matrices are defined as

$$A_{RC} = \begin{pmatrix} exp(-\frac{\Delta t}{R_1 C_1}) & 0 & 0 & 0 \\ 0 & exp(-\frac{\Delta t}{R_2 C_2}) & 0 & 0 \\ 0 & 0 & exp(-\frac{\Delta t}{R_3 C_3}) & 0 \\ 0 & 0 & 0 & exp(-\frac{\Delta t}{R_4 C_4}) \end{pmatrix}$$

and

$$B_{RC} = \begin{pmatrix} 1 - exp(-\frac{\Delta t}{R_1 C_1}) \\ 1 - exp(-\frac{\Delta t}{R_2 C_2}) \\ 1 - exp(-\frac{\Delta t}{R_3 C_3}) \\ 1 - exp(-\frac{\Delta t}{R_4 C_4}) \end{pmatrix}.$$

Δt is the sampling frequency.

The measurement equation:

$$v[k] = OCV(z[k]) - R_0 i[k] - \sum_{j=1}^{4} R_j i_{R_j}[k] + r[k]. \quad (2.25)$$

Some assumption with this model:

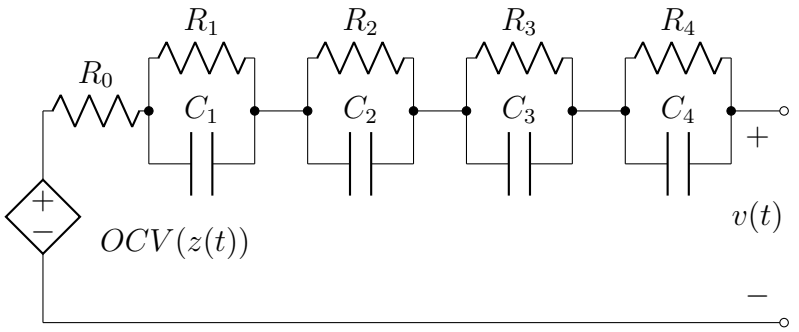

Figure 2.10: ECM with four RC circuit and a series resistance. The OCV is given as a function of SoC ($z(t)$) and the terminal voltage is denoted by $v(t)$

- Coulombic efficiency is neglected.
- Hysteresis effect is neglected.
- The $OCV(z[k])$ does not depend on temperature.

The models have to be adopted for use with the EKF and SPKF For the SPKF there is no change in the model per se, only the algorithm changes. The EKF on the other hand, requires extensive changes to linearize the model for each time step.

2.4.1 Implementing the extended Kalman filter

The linearized state and input matrices are simple to find, as the system has the form in eq. (2.24). By using the following fact [38]

$$\frac{dAx}{dx} = A$$

eq. (2.19) becomes

$$\hat{A}_k = \frac{\partial f(x_k, u_k, q_k)}{\partial x_k} = A,$$

and eq. (2.20) becomes

$$\hat{B}_k = \frac{\partial f(x_k, u_k, q_k)}{\partial q_k} = B.$$

Note that A and B are diagonal so transposing does not change the result ($A^T = A$).

The linearized output matrix, eq. (2.21), is

$$\hat{C}_k = \begin{pmatrix} \frac{\partial OCV(z_k)}{\partial z_k}\Big|_{z_k=\hat{z}_k^-} & R_1 & R_2 & R_3 & R_4 \end{pmatrix},$$

which is interesting due to the derivative of the OCV curve. It should be noted that every derivative is evaluated in the predicted point, but it is only relevant for the OCV derivative.

Finally the feed through matrix, eq. (2.22)) after linearizing is trivial and equal to

$$\hat{D}_k = 1$$

In order to find the derivative of the OCV curve, an empirical method is necessary. The following sections will start with the construction of the OCV curve, and then the derivative.

2.5 Curve fitting and derivative

There are many different methods to model the relationship between the OCV and SoC[39][40]. In this thesis, two methods have been investigated to model this relationship. Curve fitting and interpolation. The chosen method will affect the derivative of the fitted curve, and for the interpolation, it will be evident that some filtering is needed.

2.5.1 Least square and curve fitting

In order to fit a curve to a set of data, it is common to use a least square method. By assuming the structure of the fitted curve, i.e., as a polynomial of a certain order, the coefficients can be found such that the square of the residuals is minimized. By defining the residual as such

$$r_i = y_i \hat{y}_i, \tag{2.26}$$

the optimization problem can be formulated in the following manner

$$\min_{\boldsymbol{\theta}} \boldsymbol{r}^2, \tag{2.27}$$

where θ is the vector of coefficients and r^2 is a vector of the squared residuals.

By defining the *design matrix*, $\boldsymbol{X}$ where each row is a sample, and the columns match the value of the coefficients. For example, given the following samples

$$\boldsymbol{y} = \begin{pmatrix} 1 \\ 1 \\ 2 \\ 3 \end{pmatrix}$$

and the following structure

$$\hat{y}_i = \theta_0 x_i^0 + \theta_1 x_i^1 + \theta_2 x_i^2,$$

the design matrix will have the following values

$$\boldsymbol{X} = \begin{pmatrix} 1^0 & 1^1 & 1^2 \\ 1^0 & 1^1 & 1^2 \\ 2^0 & 2^1 & 2^2 \\ 3^0 & 3^1 & 3^2 \end{pmatrix} = \begin{pmatrix} 1 & 1 & 1 \\ 1 & 1 & 1 \\ 2 & 2 & 4 \\ 3 & 3 & 9 \end{pmatrix}.$$

The estimated points will then have the following equations

$$\hat{\boldsymbol{y}} = \boldsymbol{X}\boldsymbol{\beta}, \quad \boldsymbol{\theta} = \begin{pmatrix} \theta_0 \\ \theta_1 \\ \vdots \\ \theta_n \end{pmatrix},$$

and the optimization problem, eq. (2.27) can be solved [41].

2.5.2 Interpolation

Interpolation is a method that can be used to relate discrete samples to achieve a greater resolution in experimental data. There are many ways to relate the discrete points. By relating the points using functions that can be constants, linear, polynomial, or splines [42]. Depending on the sampling frequency and the frequency of the sampled process, these functions will have different effects. Usually, if the sampling frequency is high compared to the process dynamics, the chosen methods will not significantly affect the results. The relationship between the process dynamics and the sampling frequency will be further discussed in the methodology chapter.

2.5.3 Finite difference

The definition of the derivative is

$$\lim_{h\to 0} \frac{f(x+h) - f(x)}{h} \tag{2.28}$$

which is easy to use when the function to differentiate is well behaving. In the experimental data, after interpolation the function becomes a piece-wise continuous function which often can contain small sharp changes which can make the derivative very noise.

A solution is to use the finite difference method. Instead of letting $h \to 0$ it is instead chosen as a finite value $h \to \Delta h$. By defining one of the three following differences

- Forward difference $\Delta_h[f](x) = f(x+h) - f(x).$
- Backward difference $\nabla_h[f](x) = f(x) - f(x-h).$
- Central difference $\delta_h[f](x) = f\left(x + \frac{h}{2}\right) - f\left(x - \frac{h}{2}\right).$

which can be related to the derivative eq. (2.28) with [43]

$$\lim_{h\to 0} \frac{f(x+h) - f(x)}{h} \approx \frac{\Delta_h[f](x)}{h}. \tag{2.29}$$

Before doing the finite difference derivative, the experimental data will usually need to be filtered, in which case a zero phase filter might be necessary. Significant noise or outliers in the experimental data might lead to differentiating noise.

The different finite difference methods are illustrated in fig. 2.11. Both forward and central difference are non-causal operations. For most cases the central difference will be the best method, except perhaps in very non-linear cases, but then again none of the methods will perform very good.

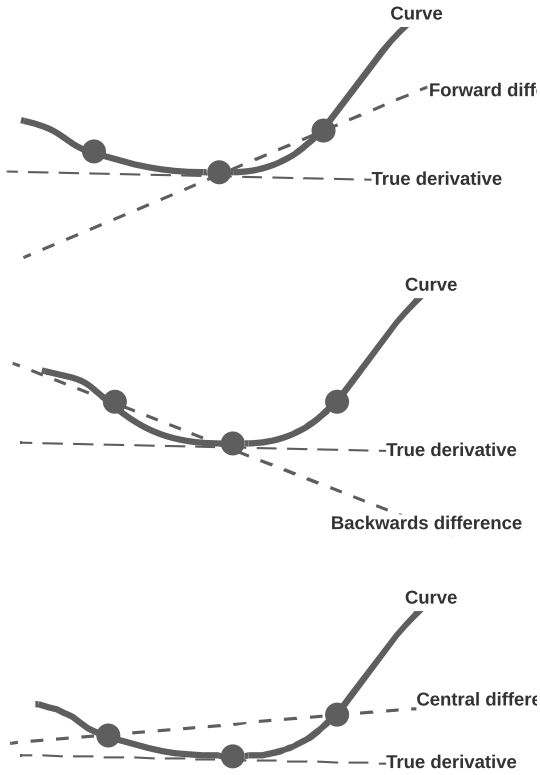

Figure 2.11: The three different finite-difference methods mentioned in this thesis.

For a time series object this can be done easily by iterating over series and calculating the difference and scaling with the sampling frequency.

2.5.4 Zero phase filtering

If collected experimental data contains some noise, the derivative will magnify the noise as conventional finite-difference approximations will greatly amplify any noise present in the data. When applying a traditional low-pass filter that will require delaying the signal for a moderate period of time, allowing the computation to predict into the future. This delay is manifested in the new signal as a phase shift. In some operations this phase shift is un-

acceptable in many applications, and for offline data there are alternatives in order to avoid this phase shift.

A popular solution is to use a zero phase filter. A method of zero phase filtering is forward-backward filtering [44]. In order to both filter the data, and keep the phase shift zero a recursive filter can be applied both forward and backwards over the signal, which would then zero out the phase shift. When applying the filter both forward and backwards, one can think of the forward as the normal way to filter which in the z-domain can be denoted $H_f(z)$ and the backwards filtering becomes the flipped filter $H_b(z) = FLIP(H_f(z))$. The flipped filter signal is $FLIP(x) = X(z^{-1})$ [44] so that the combined filtering can be written as

$$Y(z) = H(z^{-1})[H(z)X(z)]. \tag{2.30}$$

If the filter is further constrained to real filters eq. (2.30) can be written using the Fourier transform

$$Y(e^{j\omega}) = H(e^{-j\omega})[H(e^{j\omega})X(e^{j\omega})] = |H(e^{j\omega})|^2 X(e^{j\omega})$$

which shows that the filter is purely real-valued, i.e. its phase is zero and consequently there are no phase distortions.

Chapter 3

Methodology

This chapter summarises the foundation for how the experiments are set up. It starts with the models being used and how it is derived if relevant. Next, the test data in use is described, and finally, the implementation and performance measurement of the Kalman filters are introduced.

3.1 Model

In this section, the construction of a ground truth of the SoC will be presented. The OCV curve and its derivative and finally the choice of model.

3.1.1 Ground truth

In order to quantify the performance of the filters, a ground truth was established for the SoC. Although it is not strictly necessary [45], it makes the validation easier [30].

In order to construct the ground truth, the `cumtrapz` method in Matlab was used. It uses a Trapezoidal integration scheme. By using the voltage

at the end of the relaxation phase, before the load cycle starts, a initial SoC was found using the inverse of the SoC to OCV relationship.

Using this method to find the ground truth is doable in this case because it is done on offline data. With a accuracy of 0.1%chapter A gives a maximum error of $30mA$. If one assumes that the noise, to some degree, has a zero mean, the total error will be minimal when doing coulomb counting. Once the shape of the curve has been found, it can be shifted with an offset, such that it matches the experimental data quite well [46].

3.1.2 Open Circuit Voltage

Two methods for creating a static relationship between the SoC and OCV were attempted. Common for both was to first preprocess the experimental data by averaging multiple runs. The results can be seen in fig. 3.1. All of the data is performed at the same temperature, $25 \deg C$, and with such small currents, there is no temperature increase. There is some difference between the maximum and min mum data, which is because a constant current, even though small, will still cause some voltage drop, which makes the cells lower cut-off voltage trigger before the SoC reaches zero. Some of it can also be attributed to the hysteresis [47]. For details about the experiment, see [10].

Averaging the data series had the beneficial side effect of smoothing some noise. For the first method, using the least square method to fit a polynomial of order 10 to the data with the Matlab Curve Fitting toolbox [48]. A weights vector for the points was added, where the start point $(0, 3)$ and en point $(1, 4.2)$ had a slightly higher weight. For the actual implementation, the values were precomputed and put in a LUT.

Another common way to solve some of the issues related to modelling the OCV is to contract the operating area somewhat. In this thesis, the operat-

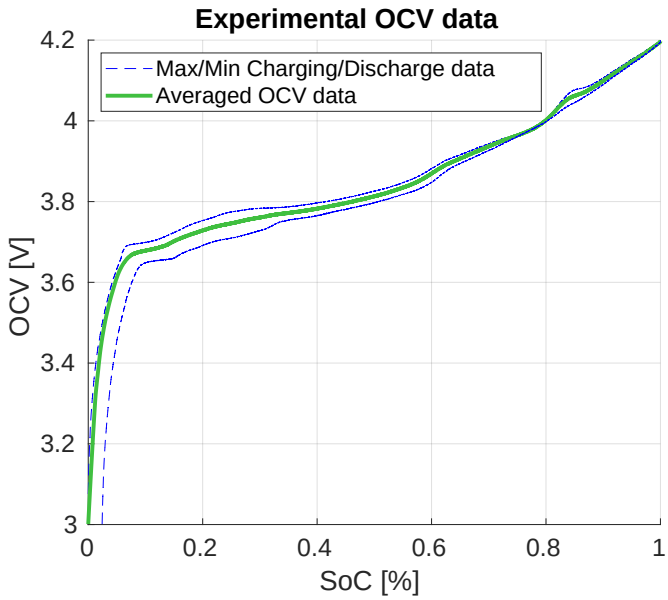

Figure 3.1: Experimental OCV data.

ing area of the SoC has been set to 2.5% to 97.5%. This solves two issues: extrapolating both solutions mentioned above is far from ideal, and the second issue is that the physical phenomenon is particularly non-linear at its endpoints [23].

In order to validate the different methods, a pre-tuned filter is run with the three different methods. It should be mentioned that ideally, the filter would be tuned optimally for each OCV data, but this is practically infeasible.

After running the filter with the different methods, the resulting SoC estimate is compared to the ground truth. Since the ground truth does not contain the initial SoC the truth is shifted vertically in order to minimize the error.

3.1.3 Choice of model

Several different equivalent circuit models were created in the previous work, and their parameters were identified. All the models were built on one or more resistor-capacitor circuits in parallel, where the numbers varied from one to four. The other main difference was whether or not they included a hysteresis effect. The performance increase from including hysteresis did not amount to much. Therefore these models have been abandoned due to the complexity of the hysteresis model.

When adding more resistor-capacitor circuits, the complexity of modelling does not increase particularly. Moreover, the added computational power needed is still reasonably small given a state vector of size two or five. The complexity is about $O(n^3)$ [49] where n denotes the size of the state vector.

The temperature has been dropped due to insufficient data for accurately modeling it.

3.1.4 Parameters

The 4-RC model has the following nine parameters:

- R_0 - Ohmic resistance
- $R_1 - R_4$ - Dynamic resistances
- $RC_1 - RC_4$ - Dynamic time constants

Where each of them contains 14 evenly spaces values across the SoC specter, which are linearly interpolated. The state vector contains the SoC as well

as the current in each resistor-capacitor circuit:

$$\boldsymbol{x} = \begin{pmatrix} z \\ i_{R_1} \\ i_{R_2} \\ i_{R_3} \\ i_{R_4} \end{pmatrix} \tag{3.1}$$

3.2 Test data

The data set used to tune and validate the filters can be seen in fig. 3.3. It contains pulses that have been adopted from actual race data performed by Revolve NTNU during a competition in Germany. The first 3 pulses have no kinetic energy regeneration, as the polarizing voltage causes the cell voltage to exceed the maximum allowed.

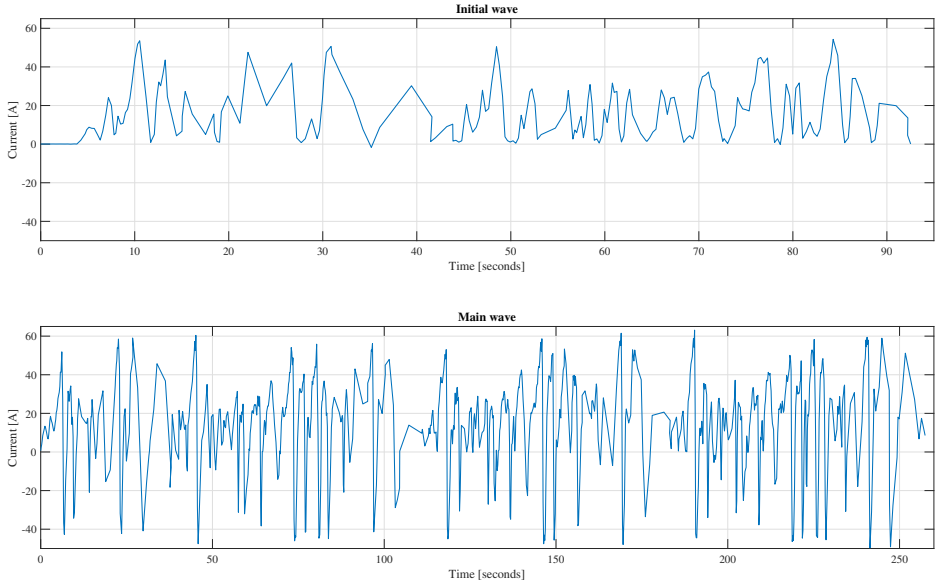

Figure 3.2: Load cycles used in the dynamic test.

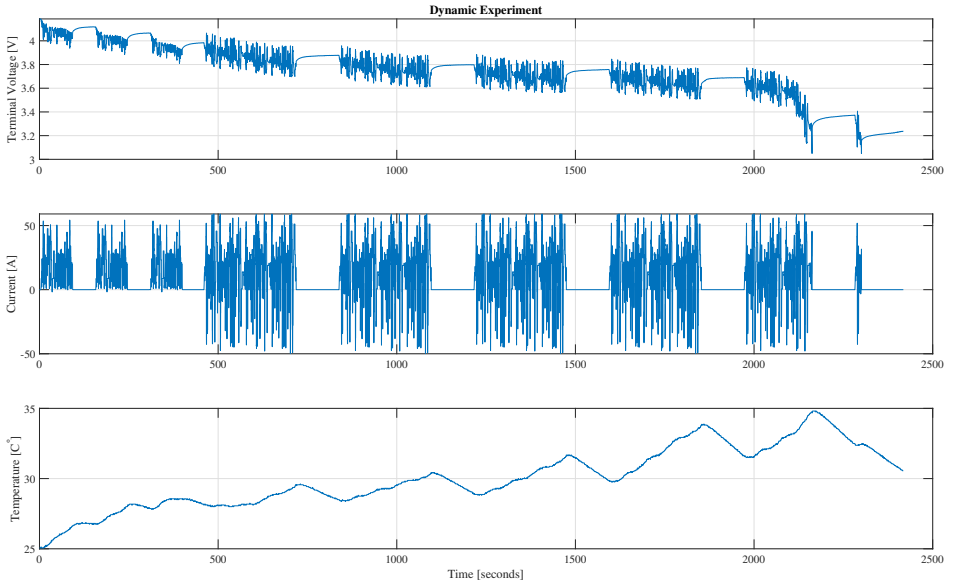

Figure 3.3: Data from a dynamic experiment. First, the three initial waveforms can be observed, which reduce the SoC. Once the SoC is at a safe level, the main waveform is applied until the SoC is ≈ 0. A short resting period between the waveforms has been added to reduce the heat generation and see how well the relaxation phase is modelled.

3.2.1 Upsampling

Early experimenting showed a slight delay in the Kalman filter output. In order to amend this, the input signals were upsampled by a factor of 2, which simulates that the filter runs at 100 Hz. The difference can be seen in fig. 3.4. The number of samples in the time series was doubled, and the last element was removed to avoid extrapolation. Then the new elements were linearly interpolated.

3.3 Filters

This section goes through the initial setup for the filters. Based on the noise, some adjustments will be made to the CDKF. A short strategy for tuning

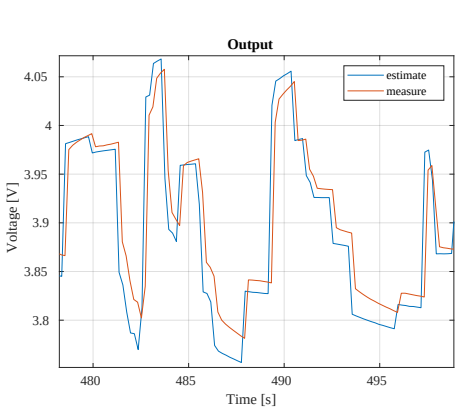

(a) Original frequency of 50 Hz.

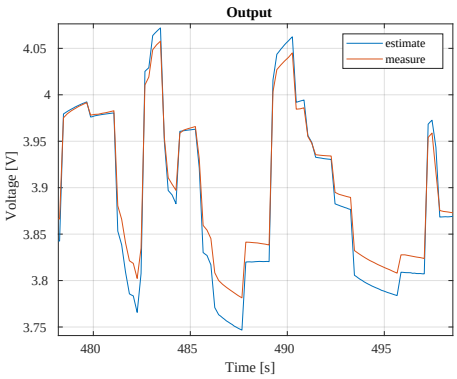

(b) Upsampled frequency which simulates 100 Hz.

Figure 3.4: The voltage output of the filters zoomed in to see the delay.

the filter and lastly, how they will be evaluated.

3.3.1 Noise and uncertainty

The EKF works optimally for Gaussian noise. The SPKF however, has a tuning factor that can determine the assumption on the noise with the tuning parameters. As mentioned in the theory section, the two most common SPKF are the unscented Kalman filter and the central-difference Kalman filter, where the UKF is more tunable and can usually be tuned better when the noise is non-Gaussian. In this thesis, the noise is assumed to be Gaussian, which will give a better basis for evaluating them against each other. Therefore the CDKF has been chosen.

With the CDKF the table table 3.1 can be used to find the weights of the sigma points when finding the new mean and covariance after the non-linear transformation.

	γ	$\alpha_0^{(m)}$	$\alpha_k^{(m)}$	$\alpha_0^{(c)}$	$\alpha_k^{(c)}$
Formula	h	$\frac{h^2-n}{h^2}$	$\frac{1}{2h^2}$	$\frac{h^2-n}{h^2}$	$\frac{1}{2h^2}$
Value	$\sqrt{3}$	$-\frac{2}{3}$	$\frac{1}{6}$	$-\frac{2}{3}$	$\frac{1}{6}$

Table 3.1: Table for the CDKF point weights.

3.3.2 Tuning

From the data sheet of the measurement equipment chapter A the initial voltage uncertainty has been set. With about 0.04% error on the 200 VDC model, the measurement uncertainty, R, has been set to 80 mV. Based on the current measurement, the process noise, Q, was set to 30 mA. However, once these were set, trial and error started. Narrowing in on the final results proved realizable with an ideology that the voltage measurements were only supposed to slightly correct the model, and the model itself would be able to track the SoC well on its own.

3.3.3 Evaluating

In order to evaluate the performance of the Kalman filters, the estimated SoC will be the primary metric. With regards to the estimated SoC the response of the system and the overall error will be important factors.

3.3.4 Timing

Matlab has a sophisticated tool for profiling the code [50], that allows for reports on how long the code runs for and how much time it spends on each line. This makes it easy to see which parts of the code take the longest and compare them.

Chapter 4

Results

This section will present the results from the two different methods of creating the OCV curve, in section 4.1. The curve fitting method on a 10th order polynomial and the linear interpolation. The derivative of the linear interpolation method was quite noisy, and therefore a second-order zero-phase filter was applied to it.

The main results are the performance of the EKF and the CDKF. In order to test them, two experiments has been ran: One in which the initial SoC is close to the actual SoC, and another where the initial SoC is set to 50%. Each filter has its own section, and the final section tries to measure the performance against each other.

fig. 4.1 demonstrates how the different results has been generated, and how the experimental data has been used.

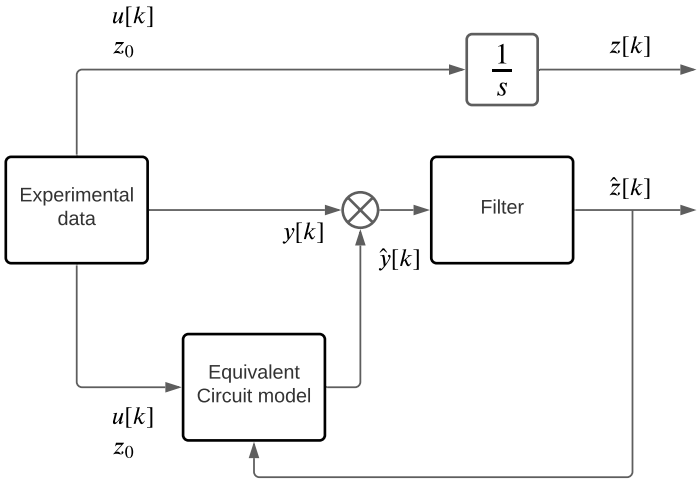

Figure 4.1: From the experimental data three quantities are retrieved, the measured voltage ($v[k]$), current ($u[k]$), and initial SoC (z_0). By exciting the model with $u[k]$ and the $\hat{z}[k]$ from the filter output, a voltage estimate ($\hat{y}[k]$) is generated. The current is integrated to create the true $z[k]$, while the filter outputs the estimate $\hat{z}[k]$.

4.1 Open Circuit Voltage

The following figures fig. 4.2 and fig. 4.3 shows the fitted curve and the interpolation with no filtering. A filtered version of the interpolation version can be seen in fig. 4.4. It is interesting to note that the same peaks on the derivative are visible on fig. 4.2 and fig. 4.3 and, to a lesser extent, the noisy one, as peaks are hard to make out at all due to the noise.

The differentiated curve is very close to zero at certain parts, especially from the $0.2 - 0.4$ SoC segment. The derivative is used as a scaling factor in the EKF, but this seems not to affect the results. The considerable rise in the derivative, as the SoC goes below 0.2, however, seems to affect the results very much on both the EKF and CDKF as will become apparent in the coming section. First, the results from using the different OCV curves

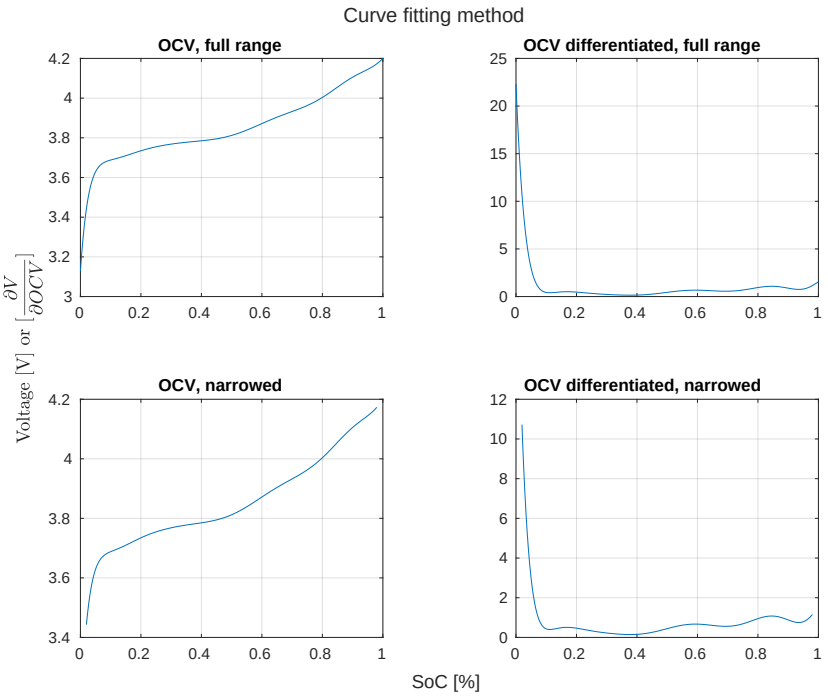

Figure 4.2: OCV and its derivative using curve fitting.

will be presented.

4.2 Derivative and filtering

In this section, the results from using different OCV curves and their derivatives are presented.

For the curve fitting where the result was a 10th order polynomial, the derivative is straightforward to find and has the nice property of being noiseless in a signal sense. If one would extend the concept of noise to also include discrepancies between the true relation between OCV and SoC it would likely contain more *noise* than the interpolated version. This noise would not be white, making the assumptions slightly worse. The assumption of white noise is not given even though the relationship was perfectly

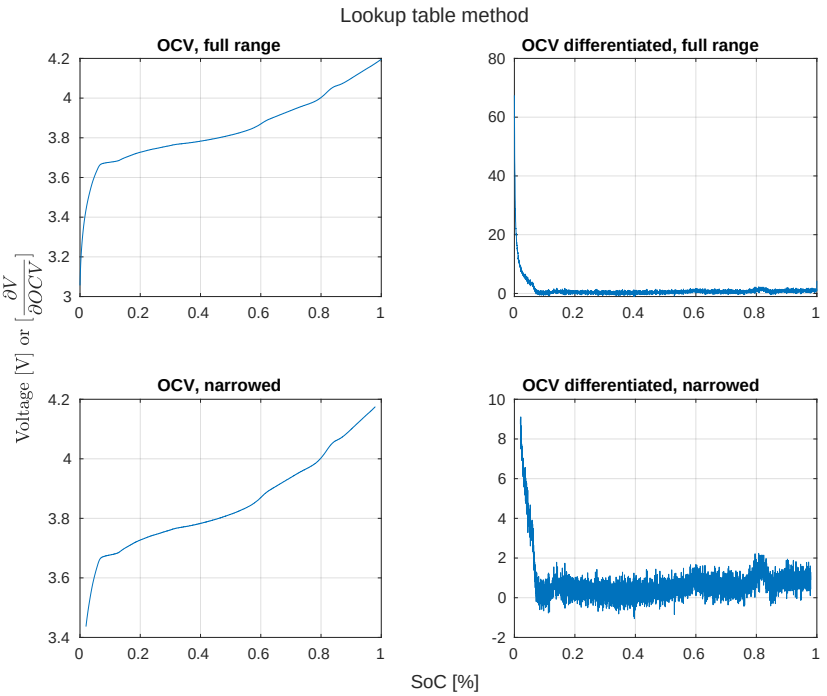

Figure 4.3: OCV and its derivative using linear interpolation.

modelled in any case. The result of a pre-tuned EKF is shown in fig. 4.5. It should also be mentioned that the fitted curve is treated as an actual function in the thesis and would naturally be turned into a LUT with pre-computed values in most use cases.

Figures fig. 4.6 and fig. 4.7 show the empirical curves with no filtering and zero-phase filtering. The effect of a noisy derivative is seen on the 3σ bound. Other than that, the estimate looks identical, which means that filtering does not assist the estimate to any great extent, but the bounds will behave better. The fact that the noise made the derivative turn negative at some points did not have any serious effect on the estimate. It should not matter regarding the updated observation covariance matrix as the Hessian of the measurement equation is squared. However, calculating the new gain matrix should affect the result. It likely made no difference due to the small

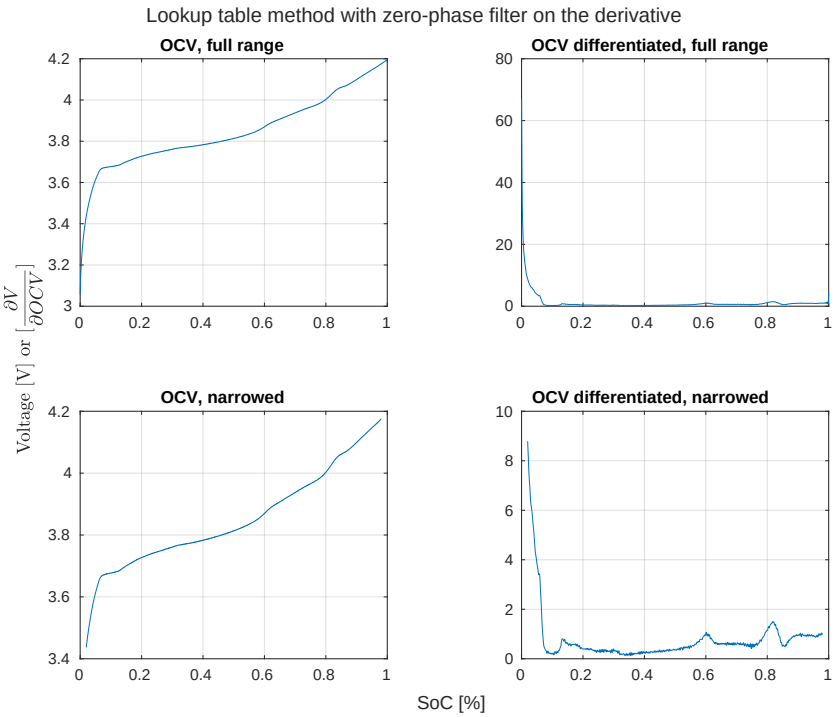

Figure 4.4: OCV and its derivative using linear interpolation. The derivative was filtered using a second-order Butterworth zero-phase filter.

magnitude, and the filter can quickly fix it in the subsequent iterations.

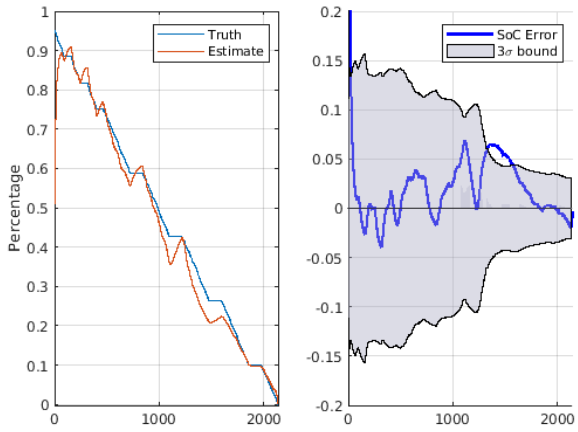

Figure 4.5: SoC and its error with 3σ bound. This is with the fitted curve and analytical derivative.

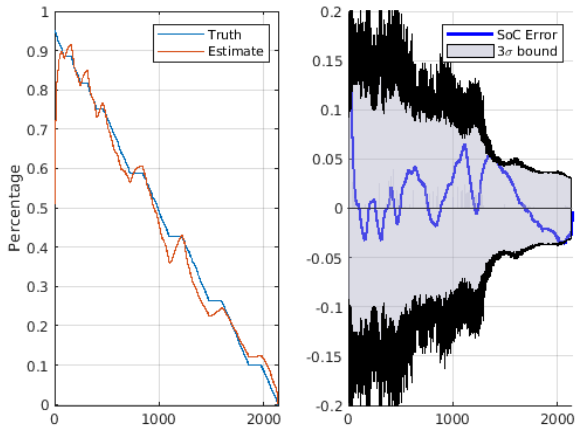

Figure 4.6: SoC and its error with 3σ bound. In this version a interpolation between the measured points have been used with a finite difference derivative.

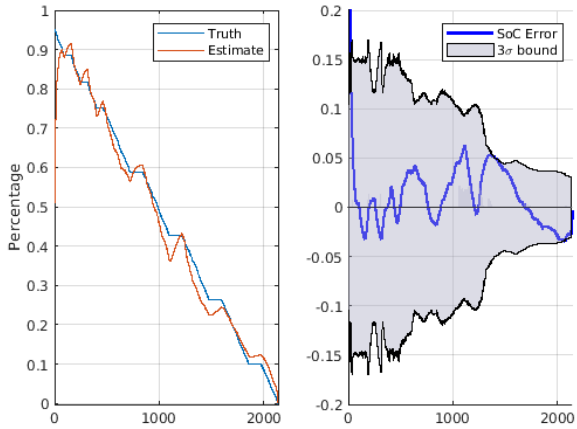

Figure 4.7: SoC and its error with 3σ bound. In this version a interpolation between the measured points have been used with a finite difference derivative. The derivative has in addition been treated with a zero-phase filter to remove some noise.

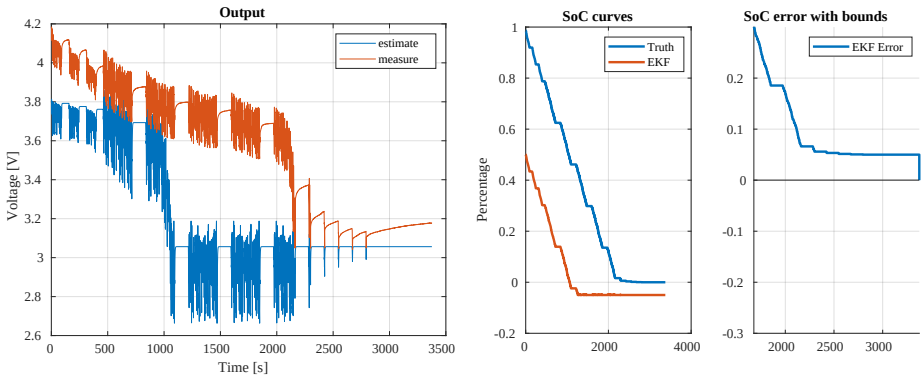

(a) Voltage output **(b)** SoC output

Figure 4.8: The output of the model with a 50% initial SoC

4.3 Model results

This section is structured first to show how the model alone is inadequate given a wrong initial SoC. It then moves on to present the result of the EKF, the CDKF and finally some comparisons between the Kalman filters.

4.3.1 No filtering

In fig. 4.8 the results of the model without any Kalman filtering are shown. Clearly, the results are not satisfactory unless the initial SoC is known, which in general will not be the case. An interesting fact with this plot is that the load pulses seem to be way off for the three last pulses. This is due to the increase in the resistor parameters as the SoC decreases [51].

4.3.2 Extended Kalman filter

All the EKF results have been conducted using the LUT solution for the OCV as well as the filtered derivative.

The SoC estimate using a good initial guess is shown in fig. 4.9. Here the initial guess is within 2% of the actual SoC. On the left right of the figure, the estimated SoC can be seen together with the ground truth. In many of the load phases, the filter seems to exaggerate the used energy, and the relaxation phase gives the battery time to approach the actual OCV which fixes the drift. This is of course not optimal and suggests that the filter should trust the model more than the voltage measurements. However, when tuning the filter, weighing the current measurements more, and decreasing the uncertainty of the initial SoC sort of pivoted the estimated curve counterclockwise.

Another part of the figure is the SoC error with its bounds. It is clear from the graph alone that the error has a non-zero autocorrelation. This is another issue with the system. If the problem is perfectly filtered, the remaining noise should be white. Nevertheless, the error at least seems to be zero-mean.

The second result related to the good guess is the output of the full model with the filter. The left side of fig. 4.9 shows the estimated voltage.

There is not too much interesting with this result, as the goal is to estimate the SoC. At the lower voltage, the discretization of the LUT can be seen. The peaks are overestimated by the filter and model, which could be either that the model parameters are wrong. That is, the resistor values and time constants. Alternatively, it could be that the resistor-capacitor currents are exaggerated by the EKF. In the relaxation phases between the loads, the filter does an excellent job of tracking the voltage. However, by looking at both the SoC estimate and the output, it seems that the relaxation phase,

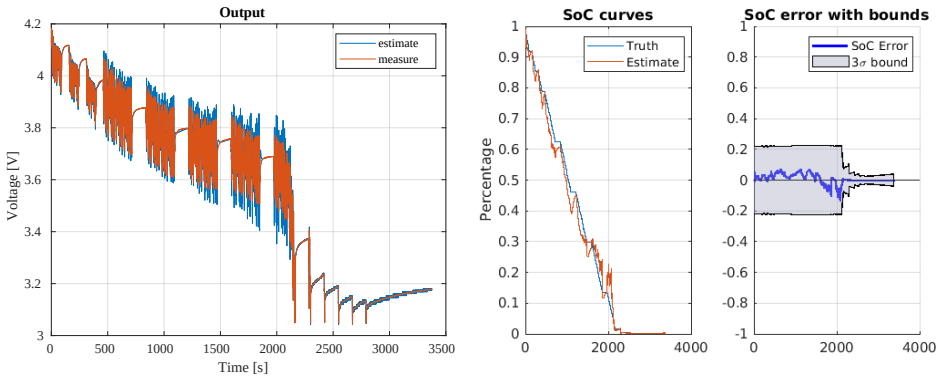

(a) The voltage output.

(b) The estimated SoC.

Figure 4.9: Results of EKF with a good initial SoC.

where the SoC should be constant due to no current flowing in or out, still changes in the estimate. This suggests that resistor-capacitor circuits do not model the polarizing voltages well enough, and the EKF has to do that part as well.

The previous work trained the model parameters using Hybrid Pulse Power Characterization (HPPC) [10]. These have relatively short relaxation phases between the pulses, which might cause the model to fail with such long relaxation phases. The HPPC used 20 seconds between the pulses, while the pauses between the load cycles are about 5 minutes.

In the next experiment the initial SoC was set to 50% and as seen in fig. 4.10 the EKF does a great job of correcting the initial error after about 5 minutes. When tuning the filter, it turned into a compromise between how fast it corrects the initial and how much it diverges at the 2000 seconds mark. This will be expanded more on in the SPKF section, as this problem is even

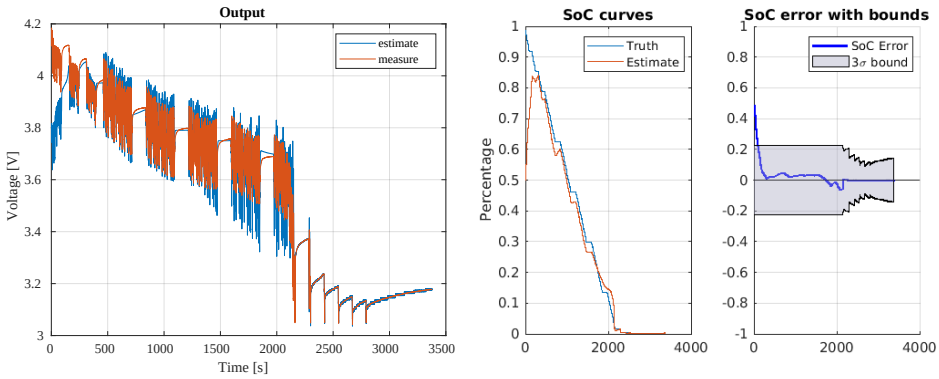

(a) The voltage output.

(b) The estimated SoC.

Figure 4.10: Results of EKF with a bad initial SoC.

more visible with that filter.

Interestingly, the relaxation phases behave better with the bad initial guess. A natural explanation would be that the error covariance gives a higher accuracy on the SoC state due to getting better feedback when adjusting it, which makes it more difficult for the EKF to change it. However, the variance bound is shown with the good and the bad guess, which is very similar, which contradicts this.

Another observation is that in both experiments, the SoC is underestimated, or in other words, the mean of the error is positive. It is important to remember that the ground truth SoC is constructed. That means it can be wrong, especially in the offset on the y-axis of the curve, or in other words, the initial SoC of the ground truth.

The output, as can also be seen in fig. 4.10, resembles the output of the good guess reasonably well, except for the beginning where the SoC has a signif-

icant error. It seems to struggle more during the relaxation phases, which is likely due to the filter giving more confidence in the voltage measurements due to the poor model results for the first 5 minutes.

The final tuning variables can be seen in section 4.3.2. Note that the initial uncertainty for all the resistor-capacitor currents is equal. As mentioned

Parameter	$\boldsymbol{R}$	$\boldsymbol{Q}$	$\boldsymbol{x}_0, i_{R_i}$	$\boldsymbol{x}_0, z$
Value	2	$2 \cdot 10^{-2}$	5	$5 \cdot 10^{-2}$

Table 4.1: The final tuning parameters for the EKF.

in the methodology chapter, the $\boldsymbol{R}$ value can be set by using the datasheet of the measuring equipment, but only tuning the $\boldsymbol{Q}$ proved inadequate for getting a good response from the filter. In practice, the $\boldsymbol{R}$ and $\boldsymbol{Q}$ values prefer the model output over the measurement. Whenever $\boldsymbol{R}$ has tuned to less or equal uncertainty as the $\boldsymbol{Q}$ the filter changed the SoC much more and much faster. The filter fixed the polarising voltages by changing the SoC which is a unwanted behavior.

There are two things of interest for the initial uncertainty on the state vector. Namely, the high uncertainty of the resistor-capacitor currents and the low uncertainty of the SoC. It would make sense that the SoC uncertainty would have a value of $\frac{1}{6}$ such that the true SoC would always be within the 3σ bound if the initial guess was set to 0.5. It was observed that by decreasing this further, the filter would not be able to change the SoC too fast, which hindered that the filter tried to estimate polarising voltages with the SoC. For the i_{R_i}, the author suspects that it is an opposite problem here, that the peaks should decay fast, and if they do not, the filter quickly becomes unstable. At least, that was the observed behavior.

4.3.3 Central Difference Kalman filter

For the CDKF the same data set has been used and the LUT for the SoC.

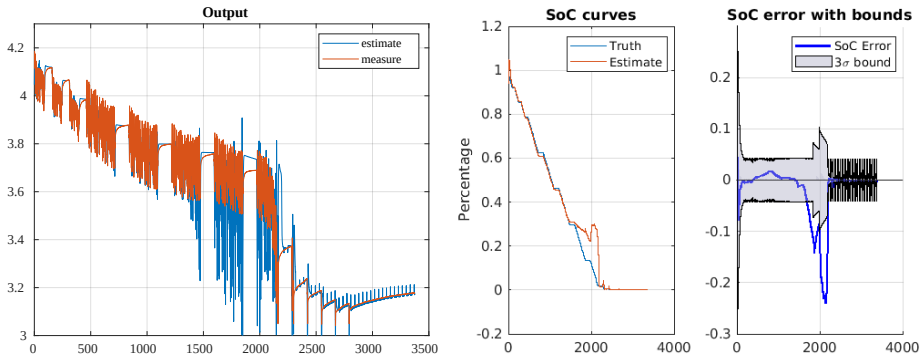

(a) The voltage output.

(b) The estimated SoC.

Figure 4.11: Results of CDKF with a good initial SoC.

In fig. 4.11 the observed behaviour of the CDKF is great until the 2000 seconds mark. As mentioned, this is a problem with both filters and is probably due to the OCV curve. What happens in the OCV curve at around 20% SoC is that the experimental data diverge the most. Additionally, the temperature starts to have a much greater effect on the OCV, as can be seen in [10]. It is therefore assumed that the error between the true OCV at this section is wrong compared to the modelled OCV.

The strange behavior of the 3σ bound jumping up is due to the Cholesky factorization of the state covariance becoming positive definite. This can happen if any of the diagonal values are negative. The ad hoc solution takes the diagonal elements' absolute value. The 3σ bound at the end is very small, which means slight numerical noise can lead to any diagonal elements becoming negative.

It looks like the filter uses only the model itself and does not use the voltage

measurements to correct the SoC, but that would mean that the SoC would be a constant in the SoC error graph. This is the optimal behavior, as the model will be able to handle the SoC well with Coulomb counting, given that the initial SoC is correct. Then the filter can simply fix the drift [6].

The output, to the left in fig. 4.11, shows a distressing problem with the SPKF. The i_{R_i} states are badly estimated and cause the voltage output estimate to be quite bad. Especially during the 2000 second mark.

With the CDKF the only interesting state becomes the SoC. It is also possible to see how the Cholesky factorization affects the results during the low SoC. This is a combination of the SoC increasing and the rapid change of the OCV at this SoC level.

The final experiment is the CDKF with a bad initial guess. The SoC can be seen in fig. 4.12. Here, as with the EKF the initial SoC has been set to 50%. After only a few seconds, the estimated SoC has stabilized, although with a bit of an overshoot. After the initial settling time, the plot is almost identical to the experiment with the good guess. This is a much quicker response than the EKF, but the CDKF suffers from the same issue that there is a compromise between how fast the response is and how well it estimates in the 2000 seconds mark. The voltage output can also be seen in fig. 4.12, but this is also identical to the previous experiment.

In table section 4.3.3 the final parameters of the CDKF can be seen.

Parameter	$\boldsymbol{R}$	$\boldsymbol{Q}$	$\boldsymbol{x}_0, i_{R_i}$	$\boldsymbol{x}_0, z$	h
Value	$2 \cdot 10^{-1}$	$2 \cdot 10^{-4}$	2	$2 \cdot 10^{-1}$	$\sqrt{3}$

Table 4.2: The final tuning parameters for the CDKF.

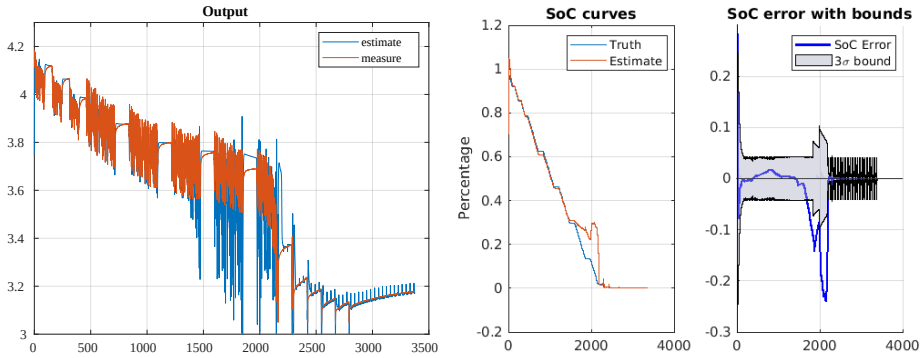

(a) The voltage output.

(b) The estimated SoC.

Figure 4.12: Results of CDKF with a bad initial SoC.

4.4 EKF versus CDKF

The results of the EKF and the CDKF can be seen in fig. 4.13. Both filters proved adequate at correcting for a wrong initial state. The CDKF responds much faster than the EKF, albeit with some overshoot. The increased response rate seems to have some unwanted side effects at the 2000 s mark.

For the timing analysis the EKF performs slightly better than the CDKF as seen in table 4.3. A lot of this can be contributed to the LUTs, as the algorithms spends about 0.3s getting one value from a LUT for the entire data series. The EKF only has to get two values, the OCV and its derivative, while the CDKF has to get 9 values (sigma points) from the OCV LUT. After correcting for this, they have very similar running time.

	Total time
EKF	5.5 s
CDKF	7.8 s

Table 4.3: The timing of the algorithm.

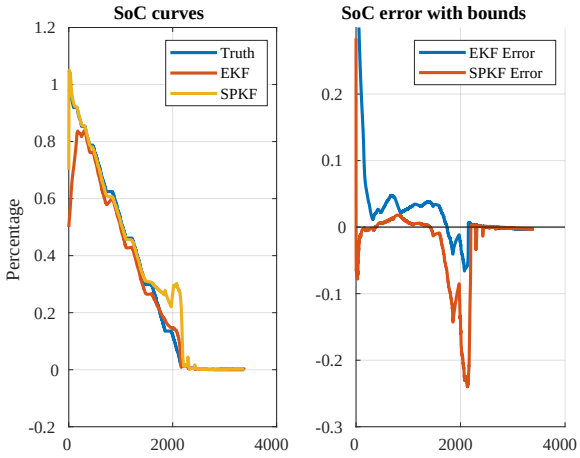

Figure 4.13: The performance of the EKF and CDKF with a bad initial guess.

Chapter 5

Conclusion

In this thesis, the problem of estimating SoC under a highly dynamic current load has been examined. The basics of battery cell chemistry and cell modelling techniques were reviewed, and a simple 4-RC ECM was developed for a model based estimation process. After a review of statistics and Bayesian estimation, the fundamentals of the EKF and two SPKF methods was presented, where the chosen SPKF was the CDKF due to fewer tuning variables.

The EKF and CDKF both showed great potential in correcting for initial SoC error, with the CDKF advancing on the correct SoC much faster than theEKF. This can probably be attributed to the tuning, as the CDKF seems more aggressive than the EKF and, as seen, overshoots and performs much worse at the start of the downwards curving of the OCV curve.

When estimating the resistor currents (i_{R_j}) the CDKF faltered, giving one the one hand much to small values, and later much higher estimates. The filtered was initially tuned to understate these resistor currents, as that gave the best results on the SoC estimation at the expense of the voltage output.

A issue was the lack of load cycle tests. More waveforms should have been generated and run in order to have multiple sets of data. This would allow multiple data sets for tuning and distinct validation sets. However, the data set used here has a demanding load, with the cell being excited quickly at almost maximum discharge and maximum charge. So in it should have an easier time estimating the SoC on less demanding loads.

Chapter 6

Further work

As this thesis is somewhat broad in the problems it tackles, this chapter will go through some of the areas where more in-depth research can be helpful.

6.1 Open Circuit Voltage

As a potentially large issue, the OCV modelling should experiment more on. One way to do this is by trying different parametric models, as done in [23], or even a non-parametric method which is done in [52]. An interesting new area is to attempt to both generate and update the OCV curve while the system runs, as in [53] online [53].

6.2 State of Charge estimation

Kalman filtering is one of many ways to estimate the SoC. In [54] the use of particle filters is investigated. A modern data-driven approach is to use neural networks, as performed in [55].

6.3 Parameter estimation

In order to expand on the BMS a useful metric to estimate is the State of Power (SoP). The SoP quantifies the maximum power possible to exert from the LIB. In order to make a good estimation of this, the SoC estimation has to be sound, as well as the impedance model [56].

In order to improve the impedance model, the EKF and CDKF can also be extended to include the parameters as states [32]. This has been performed in [57] with good results, although they do not state which chemistry the cells used.

Bibliography

[1] Gregory L Plett. *Battery Management Systems, Volume 2 Equivalent-Circuit Methods*. Boston [Massachusetts] ; London [England] : Artech House, 2016.

[2] Matlab nonlinear state estimation using unscented kalman filter and particle filter, 2017. Accessed: 2021-11-21.

[3] Habiballah Rahimi-Eichi, Unnati Ojha, Federico Baronti, and Mo-Yuen Chow. Battery management system: An overview of its application in the smart grid and electric vehicles. *IEEE Industrial Electronics Magazine*, 7(2):4–16, 2013. doi: 10.1109/MIE.2013.2250351.

[4] T.J. Mller. Lithium ion battery automotive applications and requirements. pages 113–118, 2002. doi: 10.1109/BCAA.2002.986381.

[5] Daniel H. Doughty and E. Peter Roth. A general discussion of li ion battery safety. *Electrochemical Society Interface*, jan 2012. doi: 10.1149/2.f03122if. URL `https://doi.org/10.1149/2.f03122if`.

[6] Jun Xu, Binggang Cao, Junyi Cao, Zhongyue Zou, Chunting Chris Mi, and Zheng Chen. A comparison study of the model based soc

estimation methods for lithium-ion batteries. In *2013 IEEE Vehicle Power and Propulsion Conference (VPPC)*, pages 1–5, 2013. doi: 10.1109/VPPC.2013.6671653.

[7] Dickson N. T. How, M. A. Hannan, M. S. Hossain Lipu, and Pin Jern Ker. State of charge estimation for lithium-ion batteries using model-based and data-driven methods: A review. *IEEE Access*, 7:136116–136136, 2019. doi: 10.1109/ACCESS.2019.2942213.

[8] Dominic A. Notter, Marcel Gauch, Rolf Widmer, Patrick Wäger, Anna Stamp, Rainer Zah, and Hans-Jörg Althaus. Contribution of li-ion batteries to the environmental impact of electric vehicles. *Environmental Science & Technology*, 44(17):6550–6556, 2010. doi: 10.1021/es903729a. URL https://doi.org/10.1021/es903729a. PMID: 20695466.

[9] Juan Pablo Rivera-Barrera, Nicolás Muñoz-Galeano, and Henry Omar Sarmiento-Maldonado. Soc estimation for lithium-ion batteries: Review and future challenges. *Electronics*, 6(4), 2017. ISSN 2079-9292. doi: 10.3390/electronics6040102. URL https://www.mdpi.com/2079-9292/6/4/102.

[10] Viktor Korsnes. Impedance characterisation of lithium-ion batteries. *NTNU*, 2021.

[11] Inc. The MathWorks. *Simulink Design Optimization*. Natick, Massachusetts, United State, 2021. URL https://www.mathworks.com/help/sldo/.

[12] Gregory L Plett. *Battery Management Systems, Volume 1 Battery Modeling*. Boston [Massachusetts] ; London [England] : Artech House, 2015.

[13] J. Goodenough and K. Park. The li-ion rechargeable battery: a perspective. *Journal of the American Chemical Society*, 135 4:1167–76, 2013.

[14] Kenza Maher and Rachid Yazami. Effect of overcharge on entropy and enthalpy of lithium-ion batteries. *Electrochimica Acta*, 101:71–78, 2013. ISSN 0013-4686. doi: https://doi.org/10.1016/j.electacta.2012.11.057. URL https://www.sciencedirect.com/science/article/pii/S0013468612018762.

[15] Christopher Hendricks, Nick Williard, Sony Mathew, and Michael Pecht. A failure modes, mechanisms, and effects analysis (fmmea) of lithium-ion batteries. *Journal of Power Sources*, 297:113–120, 2015. ISSN 0378-7753. doi: https://doi.org/10.1016/j.jpowsour.2015.07.100. URL https://www.sciencedirect.com/science/article/pii/S0378775315301233.

[16] Noshin Omar, Peter Van den Bossche, Thierry Coosemans, and Joeri Van Mierlo. Peukert revisited—critical appraisal and need for modification for lithium-ion batteries. *Energies*, 6(11):5625–5641, 2013. ISSN 1996-1073. doi: 10.3390/en6115625. URL https://www.mdpi.com/1996-1073/6/11/5625.

[17] Sindre Nordang. Revolve ntnu - electric race car:investigation of characteristics, cycle lifeand safety regarding lithium-ion batterycells. *NTNU*, 2016.

[18] A. J. Smith, J. C. Burns, S. Trussler, and J. R. Dahn. Precision measurements of the coulombic efficiency of lithium-ion batteries and of electrode materials for lithium-ion batteries. *Journal of The Electrochemical Society*, 157(2):A196, 2010. doi: 10.1149/1.3268129. URL https://doi.org/10.1149/1.3268129.

[19] S.S. Zhang, K. Xu, and T.R. Jow. Eis study on the formation of solid electrolyte interface in li-ion battery. *Electrochimica Acta*, 51 (8):1636–1640, 2006. ISSN 0013-4686. doi: https://doi.org/10.1016/j.electacta.2005.02.137. URL https://www.sciencedirect.com/science/article/pii/S0013468605007966. Electrochemical Impedance Spectroscopy.

[20] J. Vetter, P. Novák, M. R. Wagner, C. Veit, K. C. Möller, J. O. Besenhard, M. Winter, M. Wohlfahrt-Mehrens, C. Vogler, and A. Hammouche. Ageing mechanisms in lithium-ion batteries. *Journal of Power Sources*, 147:269–281, 9 2005. ISSN 03787753. doi: 10.1016/j.jpowsour.2005.01.006.

[21] Gert Berckmans, Lysander De Sutter, Mario Marinaro, Jelle Smekens, Joris Jaguemont, Margret Wohlfahrt-Mehrens, Joeri van Mierlo, and Noshin Omar. Analysis of the effect of applying external mechanical pressure on next generation silicon alloy lithium-ion cells. *Electrochimica Acta*, 306:387–395, 2019. ISSN 0013-4686. doi: https://doi.org/10.1016/j.electacta.2019.03.138. URL https://www.sciencedirect.com/science/article/pii/S0013468619305614.

[22] V. Pop, H. Bergveld, D. Danilov, P. Regtien, and P. Notten. *Battery Management Systems: Accurate State-of-charge Indication for Battery-powered Applications*. Springer Verlag, 2008. ISBN 978-1-4020-6944-4.

[23] B. Pattipati, B. Balasingam, G.V. Avvari, K.R. Pattipati, and Y. Bar-Shalom. Open circuit voltage characterization of lithium-ion batteries. *Journal of Power Sources*, 269:317–333, 2014. ISSN 0378-7753. doi: https://doi.org/10.1016/j.jpowsour.2014.06.152. URL https://www.sciencedirect.com/science/article/pii/S037877531401026X.

[24] Yongling He, Rong He, Bin Guo, Zhengjie Zhang, Shichun Yang, Xinhua Liu, Xichang Zhao, Yuwei Pan, Xiaoyu Yan, and Shen Li. Modeling of Dynamic Hysteresis Characters for the Lithium-Ion Battery. *Journal of The Electrochemical Society*, 167(9):090532, 5 2020. ISSN 1945-7111. doi: 10.1149/1945-7111/ab8b96.

[25] Caihao Weng, Jing Sun, and Huei Peng. A unified open-circuit-voltage model of lithium-ion batteries for state-of-charge estimation and state-of-health monitoring. *Journal of Power Sources*, 258: 228–237, 2014. ISSN 0378-7753. doi: https://doi.org/10.1016/j.jpowsour.2014.02.026. URL https://www.sciencedirect.com/science/article/pii/S0378775314002092.

[26] Mehdi Gholizadeh and Farzad R. Salmasi. Estimation of state of charge, unknown nonlinearities, and state of health of a lithium-ion battery based on a comprehensive unobservable model. *IEEE Transactions on Industrial Electronics*, 61(3):1335–1344, 2014. ISSN 02780046. doi: 10.1109/TIE.2013.2259779.

[27] Hongwen He, Rui Xiong, and Jinxin Fan. Evaluation of lithium-ion battery equivalent circuit models for state of charge estimation by an experimental approach. *Energies*, 4(4):582–598, 2011. ISSN 19961073. doi: 10.3390/en4040582.

[28] Analog Devices. Electrochemical impedance spectroscopy (eis) for batteries. 2020. URL https://www.analog.com/media/en/reference-design-documentation/reference-designs/CN0510.pdf.

[29] Anup Barai, Kotub Uddin, W.D. Widanage, Andrew McGordon, and Paul Jennings. A study of the influence of measurement timescale on internal resistance characterisation methodologies for

lithium-ion cells. *Scientific Reports*, 8, 01 2018. doi: 10.1038/s41598-017-18424-5.

[30] E Brekke. Fundamentals of sensor fusion: Target tracking, navigation and slam. *Teaching material for future course in sensor fusion, NTNU*, 2018.

[31] Christian Robert. Machine learning, a probabilistic perspective. *CHANCE*, 27(2):62–63, 2014. doi: 10.1080/09332480.2014.914768. URL https://doi.org/10.1080/09332480.2014.914768.

[32] Simo Särkkä. *Bayesian Filtering and Smoothing*. Institute of Mathematical Statistics Textbooks. Cambridge University Press, 2013. doi: 10.1017/CBO9781139344203.

[33] William L Brogan. *Modern control theory; 3rd ed.* Prentice-Hall, Englewood Cliffs, NJ, 1991. URL https://cds.cern.ch/record/226422.

[34] J.K. Uhlmann. *Dynamic Map Building and Localization: New Theoretical Foundations*. University of Oxford, 1995. URL https://books.google.no/books?id=eJb4MgEACAAJ.

[35] Rudolph Merwe, Eric Wan, and Simon Julier. Sigma-point kalman filters for nonlinear estimation and sensor-fusion–applications to integrated navigation. *Proceedings of the AIAA Guidance and Navigation & Control Conference*, 3, 08 2004. doi: 10.2514/6.2004-5120.

[36] Simon J. Julier. The scaled unscented transformation. *Proceedings of the 2002 American Control Conference (IEEE Cat. No.CH37301)*, 6: 4555–4559 vol.6, 2002.

[37] Gregory L. Plett. Extended Kalman filtering for battery management systems of LiPB-based HEV battery packs - Part 3. State and parameter estimation. *Journal of Power Sources*, 134(2):277–292, 8 2004. ISSN 03787753. doi: 10.1016/j.jpowsour.2004.02.033.

[38] Michael Spivak. *Calculus*. Publish or Perish, fourth edition, 2008.

[39] S. Nejad, D. T. Gladwin, and D. A. Stone. A systematic review of lumped-parameter equivalent circuit models for real-time estimation of lithium-ion battery states, 6 2016. ISSN 03787753.

[40] Matthias Kuipers, Philipp Schröer, Thomas Nemeth, Hendrik Zappen, Alexander Blömeke, and Dirk Uwe Sauer. An Algorithm for an Online Electrochemical Impedance Spectroscopy and Battery Parameter Estimation: Development, Verification and Validation. *Journal of Energy Storage*, 30, 8 2020. ISSN 2352152X. doi: 10.1016/j.est.2020.101517.

[41] Norman Richard Draper and Harry Smith. *Applied regression analysis*. Wiley series in probability and mathematical statistics. Wiley, New York [u.a.], 1966. ISBN 0471221708. URL `http://gso.gbv.de/DB=2.1/CMD?ACT=SRCHA&SRT=YOP&IKT=1016&TRM=ppn+022791892&sourceid=fbw_bibsonomy`.

[42] John Trangenstein. *Interpolation and Approximation*. Springer, 01 2017. ISBN 978-3-319-69109-1. doi: 10.1007/978-3-319-69110-7_1.

[43] C. Jordan, K. Jordán, and H.C. Carver. *Calculus of Finite Differences*. AMS Chelsea Publishing Series. Chelsea Publishing Company, 1965. ISBN 9780828400336. URL `https://books.google.no/books?id=3RfZOsDAyQsC`.

[44] Alan V. Oppenheim and Ronald W. Schafer. *Discrete-Time Signal Processing*. Prentice Hall Press, USA, 3rd edition, 2009. ISBN 0131988425.

[45] Shushuai Li, Christophe De Wagter, and Guido C. H. E. de Croon. Unsupervised tuning of filter parameters without ground-truth applied to aerial robots. *IEEE Robotics and Automation Letters*, 4(4):4102–4107, 2019. doi: 10.1109/LRA.2019.2930480.

[46] Kiarash Movassagh, Sheikh Arif Raihan, Balakumar Balasingam, and Krishna Pattipati. A critical look at coulomb counting towards improving the kalman filter based state of charge tracking algorithms in rechargeable batteries. 2021.

[47] C. R. Birkl, E. McTurk, M. R. Roberts, P. G. Bruce, and D. A. Howey. A parametric open circuit voltage model for lithium ion batteries. *Journal of The Electrochemical Society*, 162(12):A2271–A2280, 2015. doi: 10.1149/2.0331512jes. URL https://doi.org/10.1149/2.0331512jes.

[48] Inc. The MathWorks. *Simulink Curve Fitting*. Natick, Massachusetts, United State, 2021. URL https://mathworks.com/help/curvefit/.

[49] Aurélien Valade, Pascal Acco, Pierre Grabolosa, and Jean-Yves Fourniols. A study about kalman filters applied to embedded sensors. *Sensors*, 17(12), 2017. ISSN 1424-8220. doi: 10.3390/s17122810. URL https://www.mdpi.com/1424-8220/17/12/2810.

[50] Inc. The MathWorks. *Matlab profiler.* Natick, Massachusetts, United State, 2021. URL https://mathworks.com/help/matlab/ref/profile.html.

[51] Jun Xu, Chris Mi, Binggang Cao, and Junyi Cao. A new method to estimate the state of charge of lithium-ion batteries based on the battery impedance model. *Journal of Power Sources*, 233, 07 2013. doi: 10.1016/j.jpowsour.2013.01.094.

[52] Luis Omar Avila, Marcelo Luis Errecalde, Federico Martin Serra, and Ernesto Carlos Martinez. State of charge monitoring of li-ion batteries for electric vehicles using gp filtering. *Journal of Energy Storage*, 25:100837, 2019. ISSN 2352-152X. doi: https://doi.org/10.1016/j.est.2019.100837. URL https://www.sciencedirect.com/science/article/pii/S2352152X19302373.

[53] Yi-Hsien Chiang, Wu-Yang Sean, and Jia-Cheng Ke. Online estimation of internal resistance and open-circuit voltage of lithium-ion batteries in electric vehicles. *Journal of Power Sources*, 196(8): 3921–3932, 2011. ISSN 0378-7753. doi: https://doi.org/10.1016/j.jpowsour.2011.01.005. URL https://www.sciencedirect.com/science/article/pii/S0378775311000772.

[54] Kristian Eggereide Roaldsnes. Exploration of nonlinearities in a lithium ion battery cell model and their impact on particle filters and nonlinear kalman filters for state of charge estimation. *NTNU*, 2018.

[55] Xiangbao Song, Fangfang Yang, Dong Wang, and Kwok-Leung Tsui. Combined cnn-lstm network for state-of-charge estimation of lithium-ion batteries. *IEEE Access*, 7:88894–88902, 2019. doi: 10.1109/ACCESS.2019.2926517.

[56] Xin Lai, Long He, Shuyu Wang, Long Zhou, Yinfan Zhang, Tao Sun, and Yuejiu Zheng. Co-estimation of state of charge and state of power for lithium-ion batteries based on fractional variable-order model. *Journal of Cleaner Production*, 255:120203, 2020. ISSN 0959-6526. doi: https://doi.org/10.1016/j.jclepro.

2020.120203. URL https://www.sciencedirect.com/science/article/pii/S095965262030250X.

[57] Gregory L. Plett. Extended kalman filtering for battery management systems of lipb-based hev battery packs: Part 3. state and parameter estimation. *Journal of Power Sources*, 134(2):277–292, 2004. ISSN 0378-7753. doi: https://doi.org/10.1016/j.jpowsour.2004.02.033. URL https://www.sciencedirect.com/science/article/pii/S0378775304003611.

Appendices

Appendix A

Chroma 17020 extracts

Model	69225-200-4	69225-500-4
Channel	4	4
Charge Mode		
Voltage Range	0-200Vdc	0-500Vdc **
Maximum Current	30A	13A
Max Power	2.5KW	2.5KW
CC Mode Accuracy	0.1% stg.+ 0.05% F.S.	0.1% stg.+ 0.05% F.S.
Current Resolution	5mA	1mA
CV Mode Accuracy	0.1% stg.+ 0.05% F.S.	0.1% stg.+ 0.05% F.S.
Voltage Resolution	5mV	5mV
CP Mode Accuracy	0.2% stg.+ 0.1% F.S.	0.2% stg.+ 0.1% F.S.
Power Resolution	0.5W	0.5W
Discharge Mode		
Voltage Range *	0-200Vdc	0-500Vdc **
Maximum Current	30A	13A
Max Power	2.5KW	2.5KW
CC Mode Accuracy	0.1% stg.+ 0.05% F.S.	0.1% stg.+ 0.05% F.S.
Current Resolution	5mA	1mA
CV Mode Accuracy	0.1% stg.+ 0.05% F.S.	0.1% stg.+ 0.05% F.S.
Voltage Resolution	5mV	5mV
CP Mode Accuracy	0.2% stg.+ 0.1% F.S.	0.2% stg.+ 0.1% F.S.
Power Resolution	0.5W	0.5W
Measurement		
Voltage Range	0-200Vdc	0-500Vdc
Voltage Accuracy	0.02% rdg.+ 0.02% F.S.	0.02% rdg.+ 0.02% F.S.
Voltage Resolution	5mV	5mV
Current Range	12A/30A	4.8A/13A
Current Accuracy	0.05% rdg.+ 0.05% rng.	0.1% rdg.+ 0.05% rng.
Current Resolution	3mA	1mA
Power Range	2500W	2500W
Power Accuracy	0.07% rdg.+ 0.07% F.S.	0.12% rdg.+ 0.07% F.S.
Power Resolution	0.3W	0.3W
Temperature Range	0-90°C	0-90°C
Temperature Accuracy	±2°C	±2°C
Temperature Resolution	0.1°C	0.1°C

Note

* 0V discharge definition and charge/discharge operation range are as *Figure 1-1* and *Figure 1-2* shown.
** Voltage range is 45-500VDC when model 500V is operated in battery simulator.

V-I operation ranges of 69225/69212 series are shown as the following table. It is drawn by the data gotten by the experiment of 5m length output wire.

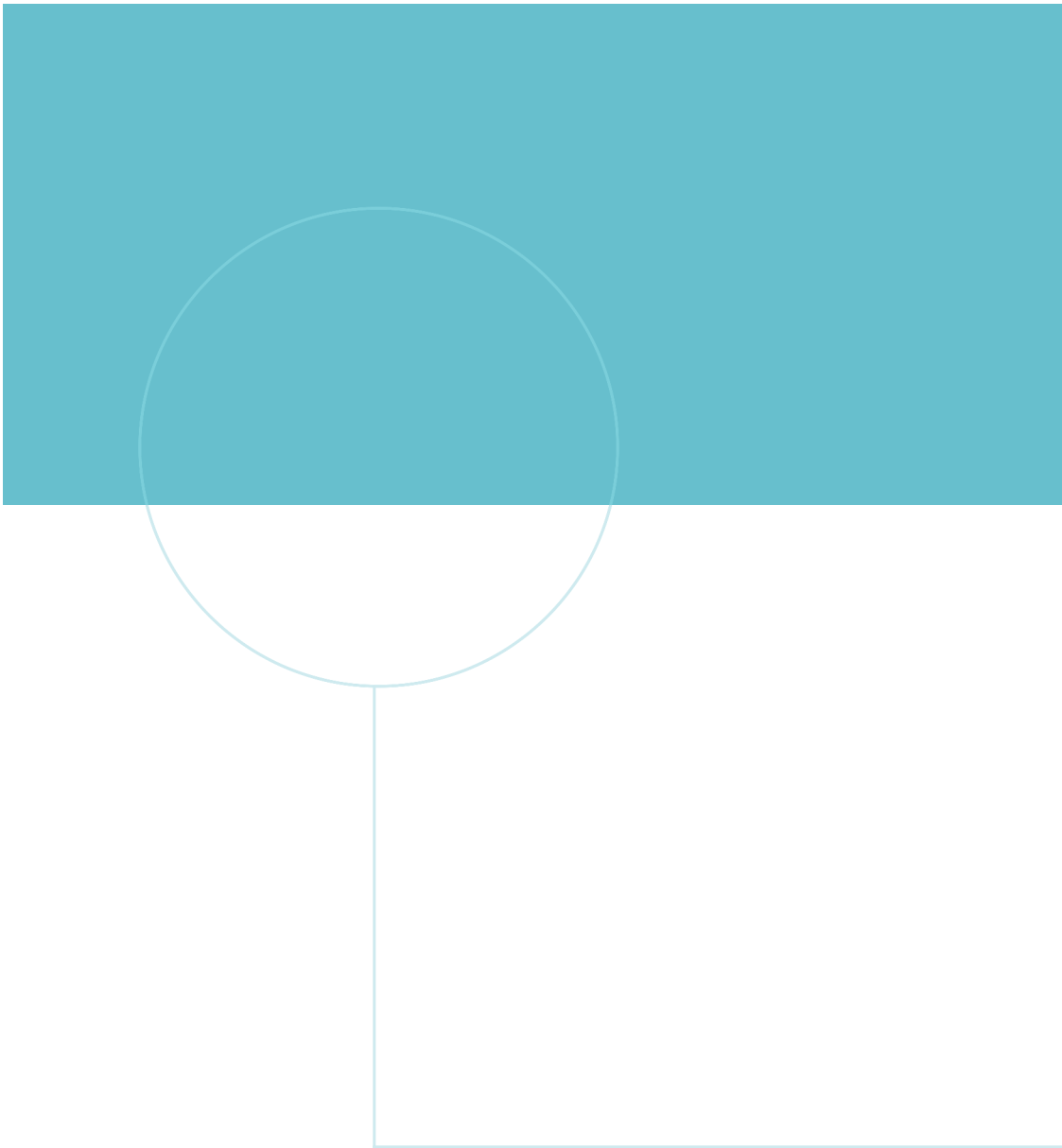

NTNU

Norwegian University of
Science and Technology